https://doi.org/10.5194/egusphere-2026-4146
Preprint. Discussion started: 23 July 2026

HERMES_Δ v1.0.1: an open-source emission processor for translating official air pollutant and greenhouse gas inventories into model-ready emissions

Marc Guevara[1], Carles Tena[1], Paula Camps[1], Kevin Oliveira[1], Johanna Gehlen[1], Angie Albarracín[1], Paula Castesana[1], Oscar Collado[1], Laura Herrero[1], Oliver Legarreta[1], Ivan Lombardich[1], Carmen Piñero-Megías[1], Luca Rizza[1], Jessica Slater[1], Artur Viñas[1], Francesca Macchia[1], Gilbert Montane[1], Oriol Jorba[1] and Carlos Pérez García-Pando[1,2]

[1]Barcelona Supercomputing Center, Barcelona, Spain
[2]ICREA, Catalan Institution for Research and Advanced Studies, Barcelona, Spain

Correspondence to: Marc Guevara (marc.guevara@bsc.es)

Abstract. This paper presents the High-Elective Resolution Modelling Emission System delta version (HERMES_Δ), an open-source, parallel and flexible emission processing tool to bridge the gap between official inventories and model-ready emissions for air quality and greenhouse gas (GHG) modelling applications. HERMES_Δ processes and combines the inventories reported to the Convention on Long-Range Transboundary Air Pollution, the EU National Emission Ceilings Directive and the UN Framework Convention on Climate Change with a large collection of detailed spatio-temporal proxies and speciation profiles to create gridded, hourly and speciated emissions for input into a variety of mesoscale modelling systems, including CHIMERE, CMAQ, MOCAGE, MONARCH and WRF-CHEM. Official emissions at sectoral and industrial facility-level of NO_x, SO_x, CO, NH_3, non-methane volatile organic compounds (NMVOC), PM_{10}, $PM_{2.5}$, black carbon (BC), CO_2 and CH_4 are combined, whereafter a detailed horizontal, vertical, temporal and speciation treatment is applied to produce ready-to-use modelling emissions compatible with multiple user-defined grids and chemical mechanisms. As a results, HERMES_Δ provides self-consistent air pollutants and GHG high resolution emissions, thus enhancing the integrated analysis of emissions affecting both air pollution and climate change. The paper exemplifies the use of HERMES_Δ by processing the Spanish official inventories and describing the methods and sources of information considered to construct the required input information, which can be used as a guidance for potential applications in other countries. Illustrations of HERMES_Δ emission outputs and of its computational performance are provided to show its capabilities. The model is designed following a flexible and transparent framework, so that it can be applicable to any European country where the required input data are available. The HERMES_Δ code is distributed through a Zenodo repository (https://doi.org/10.5281/zenodo.21393948, last access: 10/07/2026).

https://doi.org/10.5194/egusphere-2026-4146
Preprint. Discussion started: 23 July 2026

1 Introduction

The new European Ambient Air Quality Directive 2024/2881 (AAQD; EU, 2024) marks a shift in the use of air quality models for management and policy support, moving them from a complementary to a mandatory role to support assessment and planning works (EC, 2025). Out of the variety of input data and numerical parametrisations that integrate air quality models, emission inventories are recognised to be one of the most crucial as well as one of the largest sources of uncertainty in the modelling chain (de Meij et al., 2024). Therefore, a correct representation of the emission levels and their sectoral and spatio-temporal representation is essential to ensure reliability and accuracy of the modelling applications defined under the new AAQD. Concerning greenhouse gases (GHG), multiple initiatives at the national and European level are currently working on the development of observation-based GHG modelling systems. The aim of these tools is to monitor the evolution of anthropogenic CO_2 and CH_4 emissions and the impact of the mitigation policies that are being implemented to fulfil the reduction commitments established in the framework of international initiatives, such as the Paris Agreement and the European Green Deal. Examples of these systems are the Copernicus anthropogenic CO_2 and CH_4 emissions Monitoring and Verification Support capacity (CO2MVS; Janssens-Maenhout et al., 2020; Balsamo et al., 2021) or the Integrated Greenhouse Gas Monitoring System for Germany (ITMS, Gerbig et al., 2021). These GHG modelling systems combine information from in situ and satellite-based observations and from prior emission inventories with detailed Earth system models. Besides observations and models, high quality prior emission information is critical to their success (Denier van der Gon et al., 2025).

Member States under the Convention on Long-Range Transboundary Air Pollution (CLRTAP), the National Emission reduction Commitments Directive (NECD) and the United Nations Framework Convention on Climate Change (UNFCCC) are obliged to report annual national total,sectoral and point source emission inventories of air pollutants and GHG. These emission inventories are compiled following bottom-up tiered approaches as described in the EMEP/EEA air pollutant emission inventory guidebook (EMEP/EEA, 2023) and the Intergovernmental Panel on Climate Change (IPCC) Guidelines for National Greenhouse Gas Inventories (IPCC, 2019). National inventories are updated on an annual basis and go through quality assurance/quality control and verification procedures established by the Member States as well as international bodies such as the Centre on Emission Inventories and Projections (CEIP, https://www.ceip.at/, last access: 25/10/2025), which contribute to the continuous improvement of the final databases. Emissions are provided at the annual scale and contain data with a 2-year time lag, starting from the year 1990 for all species except for PM, which are only reported from the year 2000 onwards as established by the CLRTAP criteria. Air pollutant emission inventories under the CLRTAP need to also be provided in gridded form at least every 4 years following the EMEP grid, with a resolution of 0.1×0.1 degrees -approximately 10km×10km (https://www.emep.int/mscw/emep_grid.html, last access: 25/10/2025).

The compiled inventory data is used nationally and internationally to support decision making on environmental protection and to check compliance with established emission reduction commitments. However, the format in which these official

https://doi.org/10.5194/egusphere-2026-4146
Preprint. Discussion started: 23 July 2026

inventories are provided limits their usage as input for air quality and GHG modelling applications, since emissions need to be spatially resolved at a higher resolution than 10km×10km (at least 1km×1km resolution in a urban context; EC, 2025), but also temporally disaggregated to finer scales (typically hourly), vertically discretized and, in the case of lumped air pollutants (e.g., non-methane volatile organic compounds; NMVOC), chemically speciated to individual components and groups of species considered in the chemical mechanisms of air quality models.

Emission processing systems are tools that convert raw inventories into high-resolution gridded, hourly and speciated emission datasets to make them usable for model simulations. One of the most glaring examples of these systems is the open-source Sparse Matrix Operator Kernel Emissions model (SMOKE, https://www.cmascenter.org/smoke/, last access: 03/05/2026), originally designed in the late 90s to pre-process the US National Emission Inventory for fine-scale air quality modelling studies (e.g., Ma and Tong, 2022) and later on adapted for other regions of the world (e.g., Borge et al., 2008; Bieser et al., 2011). Other national tools include the Emission-MAPper tool (E-MAP; https://github.com/VITObelgium/emap, last access: 02/06/2026), designed to process the Flemish Emission Inventory. More recent examples are the High-Elective Resolution Modelling Emission System Global-Regional (HERMES_GR; Guevara et al., 2019), the Harmonized Emissions Component (HEMCO; Lin et al., 2021), the Flexible Universal processor for Modeling Emissions (FUME; Belda et al., 2024) and the Atmospheric SpatioTemporal Emissions Model (AtmoSTEM; Kakouri et al., 2026). However, in the aforementioned cases the starting point are not detailed official inventories, but emission products that are already provided in grids and sectorial aggregated forms, such as the Copernicus Atmosphere Monitoring Service (CAMS) global and European regional anthropogenic emission inventories (CAMS-GLOB-ANT; Soulie et al., 2024; CAMS-REG; Kuenen et al., 2022), which limits the specificity of the spatial proxies, temporal and speciation profiles that can be used to process them. Some chemical transport models (CTM) include dedicated emission pre-processing systems, such as the emiSURF model developed for CHIMERE (Mailler et al., 2017), the emiproc tool developed for COSMO-GHG and COSMO-ART (Jähn et al., 2020) or the Detailed Emissions Scaling, Isolation, and Diagnostic (DESID) module developed for CMAQ (Murphy et al., 2021). These systems are designed to produce emissions only compatible with their corresponding CTM, and they also consider as input already gridded and sectoral aggregated inventories.

This work presents the High-Elective Resolution Modelling Emission System delta version (HERMES_Δ), an open-access and python-based modelling tool intended for the pre-processing of the officially reported sectorial and point source level emission inventories to support air quality and GHG modelling efforts. The system combines the officially reported emission data under the CLRTAP, NECD and UNFCCC with a large collection of detailed spatio-temporal proxies and speciation profiles to adapt them to the input modelling requirements. HERMES_Δ gives the possibility to prepare emission inputs for multiple user-defined grids, chemical mechanisms and a variety of 3D mesoscale modelling systems.

https://doi.org/10.5194/egusphere-2026-4146
Preprint. Discussion started: 23 July 2026

The paper is organized as follows: Sect. 2 describes the general workflow of HERMES_Δ and the functionalities and strategies considered to perform the spatial mapping, vertical and temporal distribution and speciation treatment of the original inventories. Sect. **Error! Reference source not found.** exemplifies the use of HERMES_Δ by processing the Spanish official inventories. A detailed description of the methods and sources of information considered to construct the required input information (i.e., spatio-temporal proxies, vertical and speciation profiles) is included, so that it can be used as a guidance for potential applications in other countries. This section also presents and discusses examples of the emission outputs produced for Spain, as well as an assessment of the parallel scalability of the model. Finally, Sect. 3.3.2 presents the main conclusions of this work and future perspectives.

2 HERMES_Δ description

HERMES_Δ is an open-source emission model created and maintained by the Earth Sciences Department of the Barcelona Supercomputing Center (BSC), which builds on past experiences in the development of other versions of HERMES (i.e. Baldasano et al., 2008; Ferreira et al., 2013; Guevara et al., 2013, 2017, 2019 and 2020). The model has been developed in the framework of the high-Resolution air Emissions Systems to support modellIng and monitoRing Efforts (RESPIRE) project (https://respire.bsc.es/, last access 02/06/2026).

HERMES_Δ uses as input the officially reported annual emission inventories under the CLRTAP, NECD and UNFCCC, which need to be pre-processed to adapt them to the input format requirements of the model (see Sect. **Error! Reference source not found.**). User has the freedom to choose the sectoral (e.g., Nomenclature For Reporting, NFR; Selected Nomenclature for Air Pollution, SNAP) and spatial (e.g., NUTS level 1, 2 or 3) aggregation levels at which original emissions are provided to the model (see Sect. **Error! Reference source not found.**). The emission inputs considered by HERMES_Δ include information reported at the sectoral and individual industrial facility-level for main criteria pollutants (i.e. NO_x, CO, NMVOCs - non-methane volatile organic compounds -, SO_x, NH_3, PM_{10}, $PM_{2.5}$ and the BC component – black carbon) and GHG (i.e. CO_2 and CH_4). Unlike BC, emissions from the Organic Carbon (OC) component of $PM_{2.5}$ are not encouraged to be reported under the CLRTAP and subsequently are derived during the speciation process (see Sect. 2.5).

HERMES_Δ combines and converts the original reported emissions from specific sector categories and individual point sources into gridded, vertical, hourly and speciated emissions for input into air quality and GHG models following Eq. (1):

$$E_{out}(x, v, h, e) = \sum_{a=1}^{A} \sum_{n=1}^{N} \{E(\bar{e}) \cdot MF(x) \cdot VF(v) \cdot TF(h) \cdot SF(\bar{e})\}_{a,n} + \sum_{p=1}^{P} \{E(\bar{e}) \cdot MF(x) \cdot VF(v) \cdot TF(h) \cdot SF(\bar{e})\}_{p} \quad (1)$$

where $E_{out}(x, v, h)_e$ is the output emission of the chemical species e on the destination grid cell x, vertical layer v and hour-of-the-year h, $E(\bar{e})_{a,n}$ is the input emission of the primary pollutant $\bar{e}$ reported for the activity source a and the NUTS2 region

https://doi.org/10.5194/egusphere-2026-4146
Preprint. Discussion started: 23 July 2026

n, $E(\bar{e})_p$ is the input emission of the primary pollutant $\bar{e}$ reported for point source p, $MF(x)_{a,n}$ and $MF(x)_{p,n}$ are the emission spatial mapping weight factors to destination grid cell x associated to activity source a and region n and point source p, respectively, $VF(v)_{a,n}$ and $VF(v)_p$ are the emission vertical distribution weight factors to destination vertical layer v associated to activity source a and region n and point source p, respectively, $TF(h)_{a,n}$ and $TF(h)_p$ are the emission temporal distribution weight factors to the hour-of-the-year h associated to activity source a and the region n and point source p, respectively, and $SF(\bar{e})_{a,n}$ and $SF(\bar{e})_p$ are the speciation factors assigned to the primary pollutant $\bar{e}$, activity source a and the region n and point source p, respectively.

2.1 General workflow

Figure 1 shows a schematic representation of the structure and workflow of HERMES_Δ. The user defines general and emission sector-dependent parametrisations through the *general_configuration.ini* and *sector_configuration.yaml* files, respectively. The parametrisations include characteristics of the working domain, execution dates and input and output data paths, among others (see Sect. 2.1.1). HERMES_Δ uses this information to start the initialization process of the model, which consists of: i) the creation of the working grid where emissions will be allocated (in NetCDF and GeoJSON formats), and ii) the creation of sector-dependent spatial surrogates that are lately used to spatially map the original emissions onto the grid cells of the defined working domain. These horizontal spatial surrogates are stored as auxiliary files in NetCDF format after their creation so that they can be reused in subsequent executions. The input data files used by HERMES_Δ are divided into three main folders, which contain the pre-processed official reported emission inventories (*emission_data*), sector-dependent and general spatial proxies, including geostructures (i.e., shapefiles and GeoJSON) and raster files (*spatial_proxies*) and sector-dependent temporal, vertical and speciation profiles (*profiles*). The emission core of HERMES_Δ calculates gridded, vertical, hourly and speciated emissions in four steps that are applied to each pollutant sector and species of the original emission inventories: (i) spatial regridding (see Sect. 2.2), (ii) vertical distribution (see Sect. 2.3), (iii) temporal distribution (see Sect. 2.4) and (iv) speciation treatment (see Sect. 2.5). Once the emissions have been processed, HERMES_Δ gathers the results obtained for each sector and writes the merged data into an output NetCDF file following the requirements and conventions of the atmospheric chemistry model selected by the user (see Sect. 2.6).

https://doi.org/10.5194/egusphere-2026-4146
Preprint. Discussion started: 23 July 2026

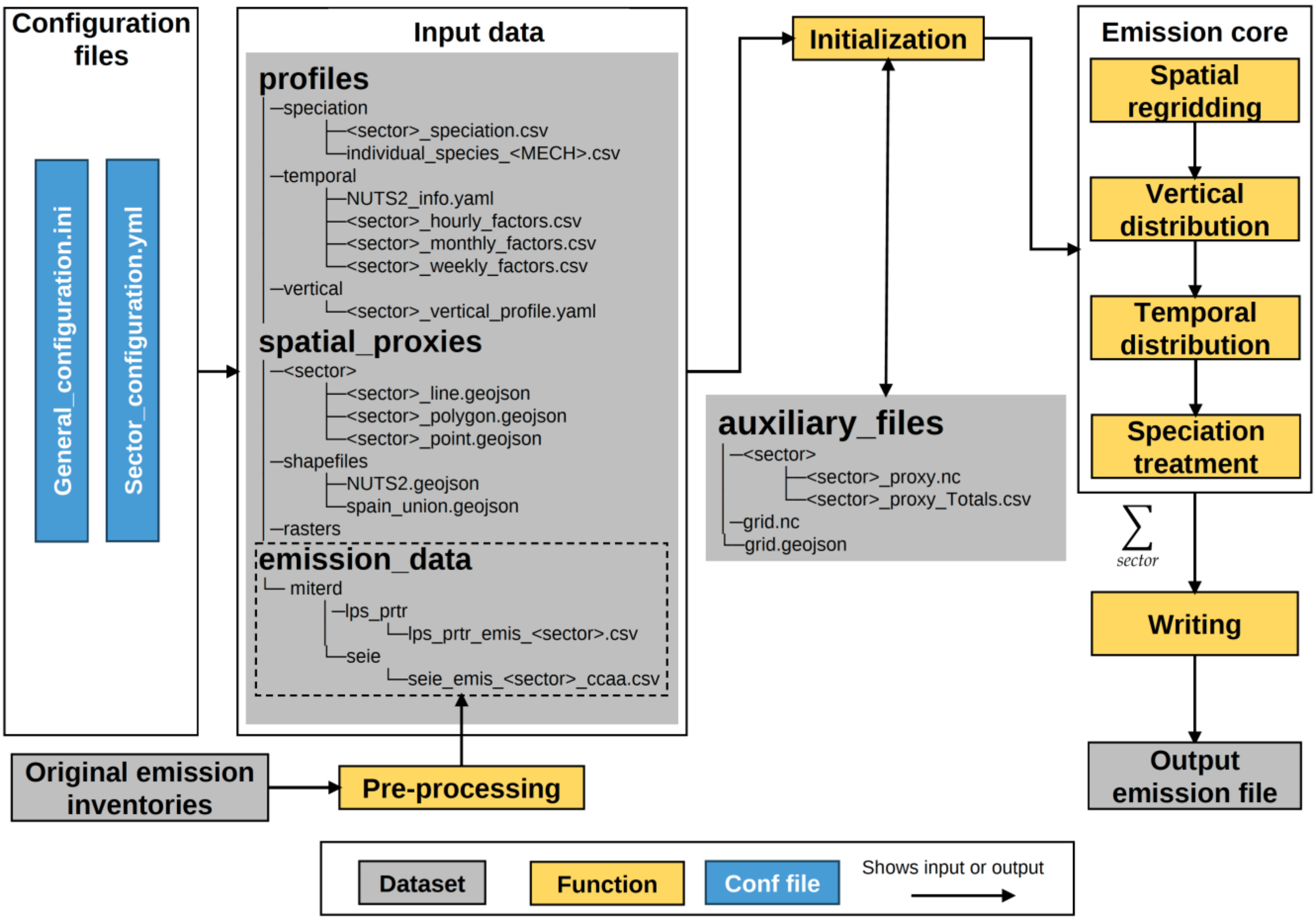

Figure 1 Schematic representation of HERMES_Δ. General and sector-dependent parameters are described by the user in the corresponding configuration files. Input data used by HERMES_Δ includes a collection of spatial proxies, temporal, vertical and speciation profiles and pre-processed official emission inventories. The information provided in the configuration files together with the input data is used by HERMES_Δ to start the initialization process, which includes the creation of working grid and of the auxiliary files. Once the general initialization is finished, HERMES_Δ starts the execution of the emission core of the model. For each sector, the model performs a (i) spatial mapping, (ii) vertical distribution, (iii) temporal distribution and (iv) speciation of the original emissions. Processed emissions are summed per grid cell, timestep and species. Once the data gathering is finished, gridded, hourly and speciated emissions are written in NetCDF format according to the atmospheric chemistry output format selected by the user.

2.1.1 Configuration files

The general and sector-dependent configuration options are passed to HERMES_Δ via the *general_configuration.ini* and *sector_configuration.yaml* files, respectively.

The *general_configuration.ini* is divided into the following sections:

https://doi.org/10.5194/egusphere-2026-4146
Preprint. Discussion started: 23 July 2026

- General: this section defines the paths to the input data, input/output directories, the name of the output emission file, time step configuration parameters (i.e. start and end dates and number of hourly time steps), the option of removing existing spatial auxiliary files at the beginning of the execution, the compression level of the output NetCDF emission file (from 0 to 9), the option of only performing the horizontal spatial distribution of the original emission inventories, the option of keeping or not a full consistency between national and point source level emissions (see Sect. 2.1.3) and the option of activating the holidays functionality, which allows HERMES_Δ to consider the impact of public national and regional holidays on the temporal distribution of emissions (see Sect. 2.4).
- Domain: this section defines the atmospheric chemistry model file convention of the resulting emission file (see Sect. 2.6), map projection (i.e., regular lat–long, rotated lat–long, Lambert conformal conic, Mercator) and characteristics of the working grid, including spatial extension, horizontal resolution and vertical description (thickness of each layer).
- Sector configuration: this section defines the path to the *sector_configuration.yaml* file.
- Common data: this section defines the paths to input data elements that are common to all emission sectors, including the georeferenced administrative borders at which emissions are originally provided (e.g., national, NUTS2 or NUTS3 level), a file defining the time zone and holiday region to which each administrative region belongs, which is used during the temporal distribution process (see Sect. 2.4), and the file that defines the mapping between individual chemical species and the chemical mechanism defined by the used, which is used in the speciation process (see Sect. 2.5).

The *sector_configuration.yaml* defines the paths to the emission input data, spatial proxies and temporal, vertical and speciation profiles associated to each emission sector.

2.1.2 Input data

The input data files used by HERMES_Δ are grouped under three categories:

- Profiles: Includes the temporal (monthly, weekly, day-of-the-year and hourly), vertical and speciation profiles used to perform the temporal (see Sect. 2.4) and vertical distribution (see Sect. 2.3) and speciation treatment (see Sect. 2.5) of the original emissions.
- Spatial proxies: Includes the georeferenced objects (i.e., GeoJSON, shapefiles and raster files) used to perform the spatial distribution of the original emissions to the destination gridded domain (see Sect. 2.2 for a detailed description of the proxies used). Spatial proxies can be provided either as vector geostructures containing custom point, line or polygon geometries with associated weighting factors, or as georeferenced raster datasets. Raster proxies may be numerical, where cell values are used proportionally during the spatial allocation process (e.g., population density), or categorical, where selected classes define the spatial distribution of emissions (e.g., land-use, crop-type or degree-of-urbanisation datasets).

https://doi.org/10.5194/egusphere-2026-4146
Preprint. Discussion started: 23 July 2026

- Emission data: Includes the emission information derived from the official sectoral and point source level inventories. Files are provided in .CSV format. Two types of files can be provided to HERMES_Δ:
    - National emission files (mandatory): Contain information on total annual emissions per pollutant, individual source category and administrative division. HERMES_Δ provides freedom to the user to choose the level of aggregation in terms of source sector classification (e.g., following the NFR, SNAP or other non-official sector classification systems) and administrative level (e.g., NUTS1, NUTS2, NUTS3) at which input emissions are provided. These files also include information on the specific spatial proxy, temporal and speciation profile that the user assigns to each source category-administrative division combination. The user also needs to indicate for which source category-administrative division combinations point source emissions are also reported, so that HERMES_Δ can perform a consistency check between the emissions provided in these files and the point source emission files (see Sect. 2.1.3). The complete list of expected fields of information is provided in Table 1.
    - Point source emission files (optional): Contain information on total annual emissions per industrial facility at their exact geographical locations (latitude and longitude). These files also include information on the specific stack height, and temporal and speciation profile that the user assigns to each point source. Each point source can be individually activated/deactivated by the user setting their corresponding CONS field to 1/0. The complete list of expected fields of information is provided in Table 2.

Official emissions as reported in the open-access national inventory submissions under the CLRTAP (https://www.ceip.at/webdab-emission-database, last access: 10/06/2026), NECD (https://cdr.eionet.europa.eu/es/eu/nec_revised, last access: 10/06/2026) and UNFCCC (https://unfccc.int/topics/mitigation/resources/registry-and-data/ghg-data-from-unfccc, last access: 10/06/2026) need to be pre-processed and adapted to the input format requirements of HERMES_Δ (as defined in Table 1 and Table 2). This pre-processing step takes place outside the HERMES_Δ model. The rationale behind this decision is that while the national inventory submissions need to follow specific reporting formats and templates, in many cases national emission inventory agencies internally compile these inventories with a larger granularity and level of detail, following standards and templates that are not homogeneous across countries. For instance, in the case of Spain, the inventory reported by the Ministry for the Ecological Transition and the Demographic Challenge (MITECO) under the CLRTAP, which need to be provided at the national level and following the NFR nomenclature, is originally compiled at NUTS2 level (17 autonomous communities – CCAA, and 2 autonomous cities) and following a sector classification system that goes beyond the categories contemplated in NFR (e.g., emissions split per fuel and crop type).

https://doi.org/10.5194/egusphere-2026-4146
Preprint. Discussion started: 23 July 2026

Table 1 List of fields of information provided in the national emission input file, including name of the column, data type (srt: string, bool: Boolean, float64: double-precision floating-point format) and description.

Column Name	Type	Description
Source_category_description	str	Individual alphanumeric code associated to each emission source category (e.g., SNAP, NFR nomenclatures) (optional)
Source_category_code	str	Description of the emission source category
is_point_source	bool	Whether this source category-administrative division combination includes emissions from point source listed in the Point Sources Emission File (see Table 2) or not (`True` or `False` / `1` or `0`)
Admin_division_name	str	Name of the administrative division (optional)
Admin_division_code	str	Code of the administrative division (e.g., NUTS nomenclature; https://en.wikipedia.org/wiki/Nomenclature_of_Territorial_Units_for_Statistics, last access: 10/06/2026)
CONS	bool	Whether emissions for each source category-administrative division combination are considered or not (`True` or `False` / `1` or `0`)
spatial_proxy	str	Name of the spatial proxy to use for the horizontal mapping of the emissions from each source category-administrative division combination (must match the name provided in the *sector_configuration.yaml* file)
proxy_code	str	For those spatial proxies classified into multiple categories or level (e.g., land use type, crop type, degree of urbanisation), this field defines the category(ies) to be considered
P_month	str	Monthly temporal profile ID cross-referenced with the CSV file where the numeric monthly temporal profile weight factors are stored.
P_week	str	Weekly temporal profile ID cross-referenced with the CSV file where the numeric weekly temporal profile weight factors are stored.
P_hour	str	Hourly temporal profile ID cross-referenced with the CSV file where the numeric weekly temporal profile weight factors are stored.
P_day	str	Day-of-the-year temporal profile ID cross-referenced with the CSV file where the numeric weekly temporal profile weight factors are stored. (optional; mutually exclusive with `P_month` + `P_week`)
P_spec	str	Speciation profile ID cross-referenced with the CSV file where the speciation profiles are stored.
P_vert	str	Vertical profile ID cross-referenced with the CSV file where the vertical profiles are stored.
`<pollutant>`	float64	One or more columns, each representing the annual emissions associated to a specific air pollutant or greenhouse gas in t/year (e.g., nh3, co, nmvoc)

https://doi.org/10.5194/egusphere-2026-4146
Preprint. Discussion started: 23 July 2026

Table 2 Same as Table 1, but for the point source emission input file

Column Name	Type	Description
Code	str	Unique alphanumeric identifier of the point source (optional)
Name	str	Name of the point source (optional)
Latitude	float64	Latitude of the emission point in WGS84
Longitude	float64	Longitude of the emission point in WGS84
Source_category_description	str	Description of the emission source category (optional)
Source_category_code	str	Individual alphanumeric code associated to each emission source category (e.g., SNAP, NFR nomenclatures)
Admin_division_name	str	Name of the administrative division where the point source is located (optional)
Admin_division_code	str	Code of the administrative division where the point source is located (e.g., NUTS nomenclature; https://en.wikipedia.org/wiki/Nomenclature_of_Territorial_Units_for_Statistics, last access: 10/06/2026)
CONS	bool	Whether emissions from each point source are considered or not (`True` or `False` / `1` or `0`)
Stack_height	float64	Altitude of the stack associated to the point source (in m)
plume_rise_factor	float64	Factor to account for the vertical rise of the industrial plume. This factor multiplies the stack height value provided under stack_height to estimate an effective emission height and perform the vertical distribution (see Sect. 2.3)
P_month	str	Monthly temporal profile ID cross-referenced with the CSV file where the numeric monthly temporal profile weight factors are stored.
P_week	str	Weekly temporal profile ID cross-referenced with the CSV file where the numeric weekly temporal profile weight factors are stored.
P_hour	str	Hourly temporal profile ID cross-referenced with the CSV file where the numeric weekly temporal profile weight factors are stored.
P_day	str	Day-of-the-year temporal profile ID cross-referenced with the CSV file where the numeric weekly temporal profile weight factors are stored. (optional; mutually exclusive with `P_month` + `P_week`)
P_spec	str	Speciation profile ID cross-referenced with the CSV file where the speciation profiles are stored.
`<pollutant>`	float64	One or more columns, each representing the annual emissions associated to a specific air pollutant or greenhouse gas in t/year (e.g., nh3, co, nmvoc)

https://doi.org/10.5194/egusphere-2026-4146
Preprint. Discussion started: 23 July 2026

2.1.3 Consistency between national and point source level emission inventories

All point and non-point anthropogenic emission sources are reported per source sector category under the CLRTAP, NEDC and UNFCCC national emission inventories (NEI). In addition, EU Member States are required to report annual emission information at the level of individual installations under the Large Point Sources (LPS) database of the NECD (https://cdr.eionet.europa.eu/es/eu/nec_revised/lps/envabhxzw/, last access: 18/05/2026) and the Industrial Emissions Portal Regulation (IEPR, https://industry.eea.europa.eu/industrial-emissions, last access: 10/06/2026). The LPS and IEPR databases only report emissions from those point sources that are above standardized reporting thresholds (e.g., production or employment capacity, annual emissions). While representing only a subset of the total national emissions included in the national inventories, the LPS and IEPR registries have the advantage of reporting emissions at the exact geographical location of each plant, increasing the accuracy of their spatial mapping.

The NEI data is consistent with the LPS data, as established by the NECD, but not necessarily with the IEPR data. This is due to the different approaches used to construct the LPS and IEPR databases, which vary among countries. For instance, in the case of Spain LPS emissions are directly estimated by MITECO making use of activity and emission data provided by the corresponding industries through surveys, while in the case of IEPR emission estimates are directly reported by the industries.

When combining the three emission databases, HERMES_Δ checks the consistency between the sum of LPS plus IEPR and the NEI. This consistency check is performed for every source category-administrative division-pollutant combination. During this process, the three following scenarios are possible, which are illustrated with a Spanish case in Fig. 2:

- The NEI is larger than the sum of LPS and IEPR: This scenario occurs when some industrial facilities are below the standardized reporting thresholds and therefore not obliged to report under LPS or IEPR. The difference between NEI and LPS plus IEPR emissions, hereinafter referred to as remainder, is distributed by HERMES_Δ using other spatial proxies, as detailed in Sect. 2.2.
- The NEI is equal to the sum of LPS and IEPR: This scenario occurs when emissions from a source sector category are fully occurring in point source facilities and all of them are above the LPS/IEPR reporting thresholds. Under this scenario, HERMES_Δ directly works with the plant-level emissions reported by LPS and IEPR and ignores the emissions reported in the NEI files (see Sect. 2.1.2).
- The NEI is lower than the sum of LPS and IEPR: Under this scenario, the user can select between two options via the general configuration file (see Sect. 2.1.1).
    - The first one is for HERMES_Δ to force a consistency between the NEI and the sum of LPS and IEPR by applying a correction factor to the original IEPR emissions, which is estimated following Eq. (2).

$$CF_{p,s,a} = \frac{NEI_{p,s,a} - LPS_{p,s,a}}{IEPR_{p,s,a}} \qquad (2)$$

https://doi.org/10.5194/egusphere-2026-4146
Preprint. Discussion started: 23 July 2026

Where $CF_{p,s,r}$ is the correction factor for pollutant p, source category s and administrative division a

- The second option is for HERMES_Δ to ignore the inconsistency and use as input the emissions resulting from the sum of LPS plus IEPR.

Under this third and last scenario, the two strategies are allowed in HERMES_Δ because there are no strong foundations that allow assuming that, for a given source category-administrative division-pollutant combination, the emissions reported by the national inventory are always more accurate than the ones reported by LPS plus IEPR, or vice versa. For a given case, the NEI may be less accurate than IEPR due to uncertainties in the methodology to distribute the industrial national fuel balance across administrative regions and industry sectors, while for another case the IEPR emissions may be less accurate due to the use of a low tiered estimation approach or uncertainties in the activity and emission factors considered. Having the two strategies available in HERMES_Δ allows the user to run sensitivity test and perform indirect evaluations when using the emissions for modelling exercises. As previously indicated, this inconsistency issue is only occurring in certain countries and works to reduce the number of occurrences in which this scenario is given are already on going. For instance, in Spain the harmonization of the NEI with the IEPR registry is part of the actions for future improvements planned by the MITECO, as reported in the 2025 submission of the Spanish Informative Inventory Report (https://cdr.eionet.europa.eu/es/un/clrtap/iir/, last access: 02/06/2026).

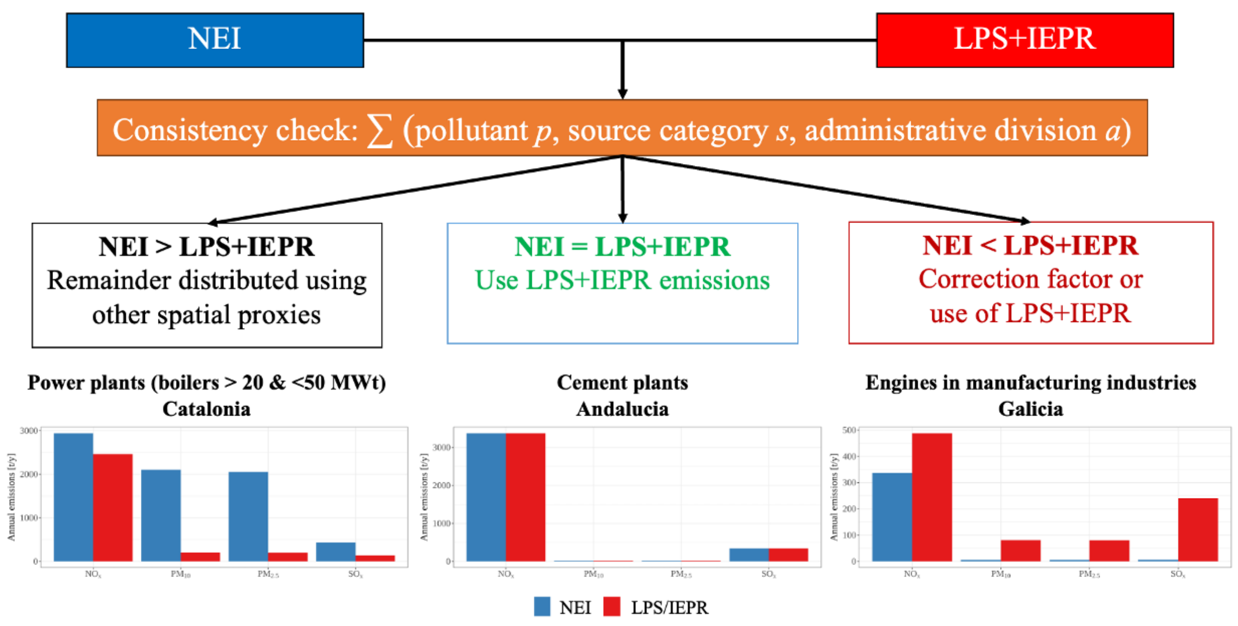

Figure 2 Schematic representation of the consistency check performed by HERMES_Δ when combining the national sectoral level (NEI) and LPS/IEPR point source level emission inventories. The consistency check is performed for every source category(*s*)-administrative division(*a*)-pollutant(*p*) combination. The scheme indicates the three possible resulting scenarios and provides an illustrative example for each one of them for Spain, where NEI (blue) and LPS+IEPR (red) annual NO_x, SO_x, PM_{10} and $PM_{2.5}$

https://doi.org/10.5194/egusphere-2026-4146
Preprint. Discussion started: 23 July 2026

emissions [t/year] are compared for the following cases (from left to right): Boilers in power plants with installed capacity between 20 and 50 MWt in the region of Catalonia (NEI > LPS+IEPR), cement plants in the region of Andalucía (NEI = LPS+IEPR) and engines in the manufacturing industry in the region of Galicia (NEI < LPS+IEPR).

2.2 Spatial distribution

HERMES_Δ can produce emissions with flexible spatial domain coverage and resolution and for several map projections (i.e., regular latitude-longitude, rotated latitude-longitude, Lambert conformal conic, Mercator), being able to cover the highest resolution at which 3D mesoscale models typically run (on the order of 1 km grid resolution; e.g., Pay et al., 2014). The spatial distribution of the emissions across the defined gridded domain is performed considering the spatial proxies assigned to each pollutant activity in the pre-processed emission input file (see Sect. **Error! Reference source not found.**) and using the latitude and longitude coordinates provided per facility for the point source emission data.

The model includes multiple functionalities for manipulating and performing spatial operations on a variety of georeferenced objects provided by the user, including point, line and polygon GeoJSON files and shapefiles and categorical and numerical raster files. Each of the elements included in a georeferenced object (e.g., discrete geographical location in the point shapefile, pixel in a raster file) must be assigned with a specific weight (e.g., installed capacity, number of inhabitants). The spatial operations are performed through a vector-based representation of both the destination grid and the input georeferenced objects, allowing the application of conservative remapping procedures between source and destination geometries.

HERMES_Δ uses the information provided in these georeferenced objects to create spatial proxies that contain the normalised fraction of emissions that goes into each grid cell of the desired working domain. For that, the following steps are executed:

- Generation of a vector representation of the destination modelling grid, where each grid cell is represented by an individual polygon.
- Conversion of all input georeferenced objects into a common vector representation and projection system.
- Application of a conservative remapping procedure to quantify the contribution of each source proxy element to each destination grid cell based on the corresponding geometric measure (e.g., area, length or point magnitude).
- Aggregation of the total proxy quantity for each administrative region.
- Normalisation of the proxy values independently for each administrative region, ensuring that the sum of all grid-cell contributions equals one.
- Storage of the resulting normalised spatial proxies in auxiliary NetCDF files for efficient reuse during subsequent simulations.

HERMES_Δ also supports the use of double proxies, which combine two independent spatial datasets during the allocation process. In this approach, a primary proxy provides the spatial distribution weights, while a secondary proxy acts as a spatial filter or scaling factor. For example, population density can be used as the primary proxy to distribute emissions, while a

https://doi.org/10.5194/egusphere-2026-4146
Preprint. Discussion started: 23 July 2026

polygon geostructure identifying municipalities connected to the natural gas network is used to restrict the allocation only to the areas where the activity can occur. This approach enables the incorporation of additional spatial knowledge when a single proxy is not sufficient to adequately represent the spatial distribution of an activity.

As the proxy calculation can be very resource intensive, spatial proxies are saved as auxiliary files, so they can be reused for any simulation with the same working domain and input georeferenced objects (see Sect. 3.3.1). For point sources, the geographical coordinates of each facility are used to identify and assign the emissions to the grid cell containing the facility within the working domain. Due to the low computational cost of this operation, the point source-to-grid-cell association is not stored as an auxiliary file.

https://doi.org/10.5194/egusphere-2026-4146
Preprint. Discussion started: 23 July 2026

2.3 Vertical distribution

Emissions are distributed across the vertical layers of the destination domain defined in the general configuration file of the model (see Sect. 2.1.1).

The user can define specific activity- and region-dependent vertical profiles, which describe the fraction of emissions released within different height intervals above ground level. These profiles are independent of the vertical discretisation of the destination domain and are provided by the user through YAML files, one per general sector, containing the alphanumeric profile identifiers that are cross-referenced with the emissions input files (see Table 1). During execution, HERMES_Δ internally maps the emissions associated with each vertical profile to the vertical layers defined in the destination domain, allocating emissions proportionally according to the overlap between the profile height intervals and the model layers. This approach allows the same vertical profiles to be reused across different modelling vertical configurations without requiring any modifications.

Point source emissions are vertically distributed considering the stack height and a plume rise factor that is associated to each individual facility, both parameters being provided by the user in the associated point source emission input file (Table 2). HERMES_Δ allocates the emissions to the vertical layer closest to the resulting injection height obtained from multiplying the two aforementioned parameters. We acknowledge the limitation of this method when compared to the use of plume rise algorithms, which allows a dynamical estimation of effective plume heights for point sources considering stack and meteorological variables (e.g., Guevara et al., 2014).

HERMES_Δ is an off-line emission model and cannot consider the variability of the vertical layer depth of air quality models based on sigma vertical coordinates. Consequently, it does not distribute the emissions to the exact sigma levels of the models (which vary slightly in time and space) but to a set of fixed vertical levels that are close to them and that are defined by the user. This assumption is in line with previous works (e.g. Guevara et al., 2019) and is assumed to be a minor source of uncertainty when compared to the large uncertainty associated with plume rise algorithms (e.g. Axelrod et al., 2025) and sector-dependent vertical profiles currently used by the air quality modelling community (e.g., Colette et al., 2025).

2.4 Temporal distribution

HERMES_Δ temporally breaks down the annual reported emissions into the hourly level combining monthly (month-of-the-year) plus weekly (day-of-the-week) plus hourly (hour-of-the-day) or daily (day-of-the-year) plus hourly temporal weight factors. Temporal weight factors are provided by the user through a collection of CSV files, one per temporal resolution and general sector, which contain information on the temporal weight factors per time step and the alphanumeric profile ID

https://doi.org/10.5194/egusphere-2026-4146
Preprint. Discussion started: 23 July 2026

associated to each profile and used for the cross-referencing. The weight factors need to sum up to 12 for the monthly scale, 7 for the weekly scale, 24 for the hourly scale and 365 for the daily scale (or 366 in case of a leap year).

For the point sources, individual profiles can be assigned to each facility, while for the national emissions the profiles can be assigned independently to each source category-administrative division combination, which allow considering the impact of different climatological or sociodemographic aspects across the country.

For each emission source, HERMES_Δ combines the corresponding monthly–weekly–hourly or daily–hourly temporal profiles to calculate a year-to-hour temporal allocation factor. Temporal profiles are evaluated in local time using the time zone associated with each administrative region, allowing the model to account for regional differences and daylight-saving-time transitions. For the monthly–weekly–hourly approach, weekly profiles are dynamically rebalanced according to the actual calendar composition of each month and year, including the number of occurrences of each weekday and, when activated, the treatment of public holidays as Sundays (see paragraph below). This procedure ensures that the temporal allocation preserves the original annual emission totals while correctly representing temporal variability at the hourly scale.

HERMES_Δ allows the user to model the effect of accounting for public holidays when temporally distributing the original annual emissions. When this option is selected in the general configuration file, HERMES_Δ identifies the days from the simulation period that are public national or regional (NUTS2 level) holidays and regards them as Sundays. In other words, holidays are forced with Sunday class day-of-the-week temporal weight factors instead of the coefficients that would correspond to that day according to the calendar. The hypothesis of treating holidays as Sundays is based on an analysis performed using long time series of electricity production and traffic congestion statistics for Spain, which reveals that the average temporal weight factors obtained for Sundays and public holidays differ by only 5% (Fig. S4). When activating the holidays functionality, HERMES_Δ recalculates the weekly rebalancing factors considering the holiday-adjusted weekday distribution, thereby avoiding deviations from the original annual emissions while preserving the intended temporal behaviour of the profiles (illustrative example provided in Fig. S5).

2.5 Speciation

The speciation of original emissions is performed following a two-step approach. In the first step, HERMES_Δ splits total NMVOC, NO_x and PM emissions into individual chemical components, while in the second steps these individual species are remapped to the gas phase and aerosol chemical mechanisms selected by the user. For those species that are not originally reported in a lumped form and that are explicitly resolved by models (e.g., CO, NH_3, CH_4), a direct one to one relationship is established.

https://doi.org/10.5194/egusphere-2026-4146
Preprint. Discussion started: 23 July 2026

Concerning the first step, individual speciation profiles can be assigned to each point source facility and activity- and region-dependent national emissions. Speciation profiles are defined by the user through sector-dependent CSV files, which contain the following information:

- Alphanumeric speciation profile ID, which is cross-referenced with the same ID assigned to each source category-administrative division combination and individual facility in the emission input CSV files, respectively (see Table 1 and Table 2)
- Name of the individual chemical substance to which original reported emissions will be mapped
- Unique identifier assigned to each individual chemical substance, as described in the open scientific literature (e.g., CAS registry; https://www.cas.org/cas-data/cas-registry, last access: 15 May 2026)
- Molecular weight of each individual chemical substance (in g/mol). For aerosol species, a value of 1 is considered as emissions are provided in mass to air quality models.
- Relative share (in mass) of the total original emission species (e.g., NO_x, NMVOC, $PM_{2.5}$) associated to each individual chemical substance (expressed in %)
- Name of the original reported emission species (e.g., NO_x, NMVOC, $PM_{2.5}$)

For each speciation profile and original emission species, the sum of the relative shares associated to each individual chemical substance should be 100%.

Regarding the second step, model and chemical mechanism dependent CSV files defined by the user are used by HERMES_Δ to perform the remapping of the individual chemical substances obtained from the first step to the corresponding gas and aerosol phase chemical species. These CSV file report, for each individual chemical substances, mole-based conversion factor to the destination chemical species. For aerosol phase species, a factor of 1 is considered to do the remapping, as emissions are provided in mass to air quality models. The columns of these files refer to the names of the destination species, which need to match the atmospheric chemistry model registry names of the emission variables. Information on the desired units of the destination species should also be provided. This information is later used by HERMES_Δ during the writing process. The unique identifier assigned to each individual chemical substance is used for cross-referencing the information provided in this file with the speciation profile files.

Although conceptually performed as a two-step process, HERMES_Δ internally combines both mappings during the initialization stage to build direct conversion factors between the original inventory pollutants and the destination chemical species, thereby avoiding unnecessary calculations during the emission processing workflow.

In its current version, HERMES_Δ allows producing speciated emissions for multiple gas phase and aerosol chemical mechanisms, including Carbon Bond 5 (CB05; Yarwood et al., 2005), Carbon Bond 6 (CB06; Yarwood et al., 2010), Regional

https://doi.org/10.5194/egusphere-2026-4146
Preprint. Discussion started: 23 July 2026

Atmospheric Chemistry Mechanism (RACM; Stockwell et al., 1997), MELCHIOR2 (Mailler et al., 2017), Community Regional Atmospheric Chemistry Multiphase Mechanism versions 1 (CRACMM1; Pye et al., 2023) and 2 (CRACMM2; Skipper et al., 2024), the fifth-generation Aerosol Module (AERO5; Binkowsk and Roselle, 2003), CARB1 (Mailler et al., 2017) and the MOCAGE aerosol module (Sič et al., 2015). Users can freely define new mappings to other existing chemical mechanisms.

2.6 Writing

HERMES_Δ produces NetCDF emission output files following the convention of several 3D atmospheric chemistry models, including CHIMERE, CMAQ, MOCAGE, MONARCH and WRF-Chem. For each model, HERMES_Δ performs the required conversion of units and inclusion of mandatory parameters and global attributes. When the user activates the option of only performing the horizontal spatial distribution of the original emission inventories, emission outputs are written following the Climate and Forecast (CF1.6) Metadata Conventions. The generation of the output files is handled by a decoupled module, which allows extending the number of output formats with minimal efforts.

2.7 Technical implementation

HERMES_Δ is implemented using Python 3.10 as a modular emission processing system following an object-oriented design. A complete list of software and Python packages required by the model is provided in the HERMES_Δ GitHub repository (https://github.com/BSC-ES/HERMES_Delta, last access: 10/06/2026).

The architecture is explicitly oriented towards extensibility, allowing new functionalities to be incorporated without modifying the core emission processing logic. A clear separation is established between Input/Output (I/O) operations related to grid creation and writing according to the target model conventions, spatial proxy generation, and the speciation and vertical distribution processes.

NetCDF I/O operations are implemented through NES (NetCDF for Earth Science), a Python library developed at the BSC-CNS that provides efficient parallel reading and writing of NetCDF datasets using domain decomposition (https://pypi.org/project/NES/, last access: 15/06/2026).

The processing workflow (Fig. 1) is structured to balance flexibility and computational efficiency. During an initial preprocessing phase, the target grid corresponding to the selected projection, domain and resolution is generated and stored as an auxiliary file for reuse in subsequent executions. Prior to the computation of spatial proxies, total proxy values are calculated for each administrative region and stored in auxiliary CSV files. These totals are required for the normalization of the proxies and ensure consistency and traceability of the spatial redistribution. Spatial proxies are then generated and normalized to a unit

https://doi.org/10.5194/egusphere-2026-4146
Preprint. Discussion started: 23 July 2026

sum within each administrative region, such that each grid cell represents the fraction of emissions assigned to that cell. The resulting normalized proxy maps are stored in auxiliary NetCDF files, with the different administrative regions represented along the vertical dimension, enabling direct reuse in later runs using the same proxies. Temporal fractions are also extracted during this phase but are kept exclusively in memory, as they are only required during the temporal disaggregation step.

During the initialization stage, HERMES_Δ performs a series of internal validation checks to ensure the structural and logical consistency of user-defined configurations, input datasets and profile definitions before the emission processing workflow is executed. For instance, all the temporal profiles defined by the user are checked to ensure that the sum of the temporal weight factors is 12, 7 and 24 for each monthly, weekly and hourly profile, respectively. Effective error messages are produced by the model when an input data file does not pass the validation check to guide users by explaining what went wrong and how to fix it. Following with the previous example, if the sum of the monthly temporal weight factors for a specific profile is not 12, HERMES_Δ will produce an error message indicating the ID of the profile that should be revised.

After preprocessing, the core transformations are applied sequentially, including chemical speciation and vertical distribution. Subsequent processing is performed iteratively by time step. For each time step, temporal disaggregation is applied, followed by spatial redistribution using the normalized proxies. The corresponding results are written to disk. This iterative processing loop avoids the generation and storage of full four-dimensional emission matrices (time × vertical level × Y × X), significantly reducing memory requirements and enabling high-resolution emission processing.

Parallel execution is achieved through a coarse-grain Message Passing Interface (MPI) domain decomposition strategy. The output domain is partitioned into independent subdomains consisting of complete rows, which are processed concurrently by different MPI processes. For raster-based proxies, a dedicated strategy is applied in which the full region of interest is extracted once, the minimal required raster window is determined, and this window is subdivided among MPI processes. This approach avoids redundant data access and preprocessing, improving both I/O efficiency and memory usage.

Software quality is supported through automated unit and integration tests executed during both installation and continuous integration workflows. To facilitate reproducibility and software adoption, HERMES_Δ is distributed through fully defined Conda/Mamba environments together with an automated installation procedure that manages dependency resolution, software installation and validation testing.

https://doi.org/10.5194/egusphere-2026-4146
Preprint. Discussion started: 23 July 2026

3 Example of HERMES_Δ usage

This section presents an example usage of HERMES_Δ for Spain. In Sect. 3.1, a detailed description of the methods and sources of information considered to construct the pre-processed emission input files, spatial proxies, temporal, vertical and speciation profiles is provided, so that it can be used as a guidance for potential applications of HERMES_Δ in other countries. Sect. 3.2 and 3.3 present examples of the emission outputs produced for Spain and an analysis of the computational efficiency of the model for a specific use case, respectively.

3.1 Pre-processing of inventories and construction of proxies and profiles

3.1.1 Emission inventory input data

We consider as starting point the officially reported Spanish annual air pollutants and GHG emission inventories produced by the MITECO under the Spanish Inventory System (SEI, https://www.miteco.gob.es/en/calidad-y-evaluacion-ambiental/temas/sistema-espanol-de-inventario-sei-.html, last access 01/06/2026), together with the industrial emission databases reported under the LPS (https://cdr.eionet.europa.eu/es/eu/nec_revised/lps/envabhxzw/, last access 18/05/2026) and the Spanish Register of Emissions and Pollutant Sources (PRTR; https://prtr-es.miteco.gob.es/, last access 02/06/2026), which is equivalent to the information provided to the IEPR. For the SEI inventory, annual emissions are collected at NUTS2 level (17 autonomous communities – CCAA, and 2 autonomous cities) and following the third level of the Selected Nomenclature for Air Pollution (SNAP) reporting system, which originally consists of 11 sectors (first level), 75 sub-sectors (second level) and 440 activities (third level). For LPS and PRTR, emissions are collected at the industrial facility level for a total of 2513 industries. The pre-processing applied to each of these three datasets is described below.

For a selection of SNAP activities, original SEI emissions are split into a fourth level, which allow classifying emissions across multiple fuel, vehicle, facility, driving pattern and crop categories, and therefore assigning them to more refined and detailed spatiotemporal proxies (Table S1). The split is performed using NUTS2 level emission information reported by MITECO (personal communication) and that is consistent with the SEI emissions. As a result of the sectorial splitting process, emissions from a total of 982 individual categories per NUTS2 level are considered as input in HERMES_Δ.

The SEI annual emission data split by NUTS2, fourth level SNAP activity and pollutant is pre-processed into individual CSV files, one per general SNAP sector (i.e., *emis_<sector>.csv* in Fig. 1). The fields of information indicated in Table 1 are added to define specific spatial, temporal and speciation profiles associated to each source category-NUTS2 combination.

Concerning the LPS and PRTR point source databases, original annual emissions are provided per industrial facility at their exact geographical locations (latitude and longitude). LPS emissions are reported consistently for all air pollutants and GHG, together with information on the SNAP activity code and stack height. On the other hand, PRTR emissions are reported

https://doi.org/10.5194/egusphere-2026-4146
Preprint. Discussion started: 23 July 2026

following the National Classification of Economic Activities (CNAE) nomenclature, with no information on the associated stack height and only for those pollutants that are above the information thresholds specified in annex II to the E-PRTR Regulation (EU, 2006).

To homogenise and merge the PRTR and LPS databases into single SNAP-dependent CSV input files, the following pre-processing steps are performed to the first one:

- SNAP code assignment: Each PRTR facility is assigned to a specific SNAP code using the information from the integrated environmental licence (AAI) of each industry. If the AAI does not provide this information, a SNAP code is assigned based on the CNAE category under which the PRTR facility is classified (Table S2).
- Stack height assignment: this information is derived from the corresponding AAI of each industry. If the AAI does not provide this information, the altitude of the stack is obtained using Google Earth elevation (Google, 2026).
- Emission gap-filling procedure: The PRTR register requires reporting emissions only of those pollutants that are above the reporting thresholds defined in Annex II of the regulation (EU, 2006). This limitation results in incomplete reported emissions data for some PRTR industries, with information missing for some pollutants. To address this gap, a gap-filling method based on CO_2 emission ratios is applied following with the approaches described in Kuenen et al. (2022) and Guevara et al., (2024). The contribution of gap-filled emissions is most substantial for CO and NMVOC, with approximately 16 % and 10 %, while for the other pollutants these contributions are residual (Fig. S1).
- Filtering: When the same industrial facility is reported in the LPS and PRTR databases (e.g., power plants), preference is given to LPS, as it is consistent with the SEI emissions (see Sect. 2.1.3). Farm facilities, waste-water treatment plants and landfills reported under PRTR are excluded, since the registry only includes a subset of these facilities (e.g., poultry and pig farms with capacities above 40.000 and 2000 heads, respectively). Emissions from these sources are spatially allocated in a consistent and complete way through the SEI inventory (See Sect. 3.1.2).

3.1.2 Spatial proxies

Table 3 summarises the main spatial proxies considered to distribute the Spanish emissions for each general SNAP sector category. A full overview of all the proxies (a total of 140) assigned to each source and corresponding references is provided in the Supplementary Material (Table S3).

For sectors dominated by point sources including energy industries (SNAP01), industrial combustion plants (SNAP03) and industrial processes without combustion (SNAP04), the LPS and PRTR databases are used as the primary source for the spatial allocation. For those cases where SEI emissions are larger than LPS plus PRTR, remainder emissions are distributed using in-house point source proxies that provides the location of the facilities not included in LPS or PRTR. When this information is not available, remainder emissions are treated as an area source and distributed considering the industrial land use information provided by the CORINE Land Cover dataset at a 250mx250m resolution (CLC; Copernicus Land Monitoring Service, 2020).

https://doi.org/10.5194/egusphere-2026-4146
Preprint. Discussion started: 23 July 2026

Emissions from commercial (SNAP0201) and residential (SNAP0202) combustion activities are distributed combining the georeferenced information on population density and associated degree of urbanisation provided by the Global Human Settlement Layer project at 1kmx1km resolution (GHSL; Schiavina et al., 2023a and 2023b). Depending on the fuel category, emissions are either distributed across urban and rural population (i.e., natural gas, LPG) or only population located in rural areas (i.e., solid biomass, coal and others), following with the results from previous monitoring and modelling studies (e.g., Navarro-Barboza et al., 2024). Specific NUTS- and fuel-dependent weight factors are combined with the original GHSL population data using the double proxy functionality of HERMES_Δ (see Sect. 2.2) to properly reflect local or regional circumstances, such as the fact that not all municipalities have access to the natural have distribution network (Fig. S2). Emissions from agricultural and aquacultural combustion plants and irrigation systems (SNAP0203) are distributed considering the location and capacity of the aquaculture facilities, the Spanish livestock farm registration and the irrigation land use information provided by CLC, respectively.

Fugitive emissions from the distribution of oil products (SNAP0504 and 0505) are mapped considering a collection of in-house point sources and polygons that provide information on the location of oil storage tanks and associated capacities, oil refinery complexes and associated capacities, oil maritime terminals and associated capacities and gas stations. Fugitive emissions from the transmission and distribution network of natural gas (SNAP0506) are mapped considering the gas pipeline network and the GHSL population layer, respectively.

For use of solvents and other products (SNAP06), a distinction is made between activities related to residential/commercial and industrial uses. Industrial use of solvent emissions are mapped to the extent of possible combining the LPS and PRTR databases with an in-house point source catalogue that includes the following categories: car repairing, boat building, dry cleaning, rubber processing, pharmaceutical products manufacturing, paint manufacturing, glues manufacturing, leather tanning and printing. The remaining industrial emissions are distributed using the CLC industrial land use information. For residential and commercial use of solvent and other products (e.g., tobacco consumption and fireworks), emissions are distributed according to the total population density information provided by GHSL.

Concerning road transport emissions (SNAP07), two main proxies are considered as a function of the driving pattern. For interurban and rural traffic emissions are mapped making use of a mosaic of georeferenced annual average daily traffic data (AADT) maps for interurban and rural roads provided by various official sources (see Table S4 for details). For urban traffic, emissions are distributed making use of the Open Street Map (OSM; OpenStreetMap contributors, 2024) dataset and considering the weighting of the OSM road categories reported by Mu et al. (2022). Population density information provided by GHSL is considered for the distribution of gasoline evaporative emissions.

https://doi.org/10.5194/egusphere-2026-4146
Preprint. Discussion started: 23 July 2026

Emissions from agricultural, forestry and industrial off-road machinery are spatially mapped considering CLC land use categories. In the case of LTO emissions from aviation we consider a polygon shapefile defining the boundaries of each airport and associated annual national and international flight operation counts. Emissions from military off-road machinery are distributed across a digitalised map of military infrastructures.

SNAP09 (waste management) emissions from municipal and industrial waste incineration as well as flaring operations in refineries are allocated using the LPS database. Emissions from urban wastewater treatment plants are distributed considering the Urban Wastewater Treatment Plants database (EEA, 2023b). Emissions related to the treatment of industrial wastewater are distributed using the CLC industrial land use category due to the lack of a detailed catalogue. Emissions linked to the management of solid waste, compost and biogas plants and incineration of dead bodies are mapped using in-house shapefiles that defines their locations and associated capacities.

Concerning agriculture (SNAP10), emissions from agricultural soils and use of fertilizers are distributed making use of the European Union Crop type Map (EUCROPMAP; D'Andrimon et al., 2021), which provides information for 19 crop types at 10m resolution based on Sentinel-1 Synthetic Aperture Radar observations for the year 2018. For those crop categories not represented in EUCROPMAP such as vineyards, fruit trees or olive groves, emissions are distributed using the CLC database. The mapping between the SEI crop categories considered as input in HERMES_Δ and the EUCROPMAP and CLC categories is provided in Tables S5 and S6, respectively. Livestock emissions related to manure management and enteric fermentation are distributed using the Spanish livestock farm registration.

Table 3 Summary of main proxies used for the spatial mapping of emissions in HERMES_Δ

Emission source	Main proxies used
SNAP01: Energy industries	- PRTR and LPS - Our own point source database (e.g., district heating plants) - CORINE land cover 2018 (industrial or commercial units)
SNAP02: Non-industrial combustion plants	- Global Human Settlement Layer – Population density map (GHS-POP) - Global Human Settlement Layer – Degree of urbanisation map (GHS-SMOD) - NUTS4-level weight factors associated to energy consumption per capita for heating purposes, natural gas availability and residential wood combustion - Livestock farm registration - Aquaculture facilities - CORINE land cover (irrigated land)
SNAP03: Industrial combustion plants	- PRTR and LPS - Our own point source database (e.g., plaster furnaces, paper mill plants) - CORINE land cover (industrial or commercial units, mineral extraction sites)

https://doi.org/10.5194/egusphere-2026-4146
Preprint. Discussion started: 23 July 2026

SNAP04: Industrial processes without combustion	- PRTR and LPS - Our own point source database (e.g., titanium dioxide and calcium manufacturing industries) - CORINE land cover (e.g., extraction sites, industrial or commercial units)
SNAP05: Fugitives	- LPS - Our own polygon, line and point source database (e.g., marine terminals, natural gas pipelines) - Gas stations - Global Human Settlement Layer – Population density map (GHS-POP) - CORINE land cover (industrial or commercial units)
SNAP06: Solvents	- PRTR and LPS - Our own point source database (e.g., inks manufacturing plants, printing industries) - CORINE land cover (e.g., industrial or commercial units, construction sites)
SNAP07: Road transport	- Interurban and rural road network with associated traffic flow per vehicle type - Open Street Map urban road network combined with Mu *et al.* (2022) road type weight factors - Global Human Settlement Layer – Population density map (GHS-POP)
SNAP08: Other mobile sources and machinery	- CORINE land cover 2018 (e.g., non-irrigated arable land, broad-leaved forest) - Our own polygon and line source database (e.g., military facilities, airports) - NUTS-3 level weight factors associated to agricultural machinery power and volume of harvested trees
SNAP09: Waste	- PRTR and LPS - Our own polygon, line and point source database (e.g., controlled landfills, composting facilities, biogas plants) - Urban Waste Water Treatment Plants (WWTP) database - Global Human Settlement Layer – Population density map (GHS-POP) - CORINE land cover (dump sites)
SNAP10: Agriculture	- European Union Crop type Map (EUCROPMAP) - Livestock farm registration - CORINE land cover 2018 (e.g., vineyards, olive groves, pastures)

3.1.3 Vertical profiles

For the industrial emissions that are treated as an area source, the SNAP-dependent vertical profiles reported by Bieser et al., (2011) are considered. For residential and commercial combustion emissions, we assume that these are occurring between 30m and 60m, in line with Grythe et al. (2019). For LTO emissions from aviation, it is assumed that 40% of emissions are occurring in the surface and 60% between 10m and 1000m, following with the results from Guevara et al. (2020). For the other activities, it is assumed that all emissions are occurring at the surface level. For point source emissions, a plume rise factor of 2 is

https://doi.org/10.5194/egusphere-2026-4146
Preprint. Discussion started: 23 July 2026

considered for all facilities, based on the results reported by Pregger and Friedrich (2009), which indicate that, on average, the effective emission height of different types of industries, including power stations, combustion plants, refineries and cement plants, among others, is approximately 2 times larger than their stack height. As previously indicated in Sect. 2.3, we acknowledge the limitation of this assumption, as the effective emission height of a point source can largely vary over time due to changes in the atmospheric stability and associated regime, as illustrated in Guevara et al. (2014 and 2020).

3.1.4 Temporal proxies

The collection of temporal profiles consists of a dataset of more than 660 profiles that were obtained from multiple sources of information, including national official statistics and other proxies, as summarised in Table 4. A complete overview of the sources of information used for each pollutant activity and associated references is provided in the Supplementary Material (Tables S7, S8 and S9).

For energy industries (SNAP01), daily and hourly electricity production statistics reported per fuel, technology and Spanish region are considered for the construction of profiles for power plants. Monthly refinery and coke production statistics are used to derive the seasonality of emissions for these two industrial sectors, the weekly and hourly profiles assumed to be flat. Concerning emissions related to central district heating systems, NUTS2-dependent monthly profiles derived from the gridded CAMS European regional temporal profiles database (CAMS-REG-TEMPO) are considered (Guevara et al., 2021 and 2025).

For non-industrial combustion plants (SNAP02), the gridded profiles as reported by CAMS-REG-TEMPO for Spain are considered to produce NUTS2- and fuel-dependent monthly profiles. Fuel-dependent weekly and hourly profiles reported by CAMS-REG-TEMPO are also considered.

For industrial combustion (SNAP03) and industrial processes (SNAP04), monthly profiles per industrial branch (e.g., chemical industry, food industry) are derived from electricity consumption statistics. For selected industrial sectors, profiles are based on monthly production statistics, including cement plants, iron and steel plants and refineries. The weekly and hourly profiles reported by CAMS-REG-TEMPO for the manufacturing industry sector are considered for all industrial sources due to the lack of more detailed information.

Concerning fugitive emissions (SNAP05), monthly profiles are primarily based on national statistics on fossil fuel extraction, production and consumption (e.g. gasoline, diesel and natural gas consumption). An exception is underground mining, for which monthly profiles are derived by industrial branch (e.g., coal extraction) using electricity consumption statistics. Weekly and hourly profiles are assumed to be flat for most activities in the absence of activity-specific temporal data.

https://doi.org/10.5194/egusphere-2026-4146
Preprint. Discussion started: 23 July 2026

For use of solvents and other products (SNAP06), a flat monthly profile is proposed for domestic activities based on Heeley-Hill et al. (2021), which indicate that usage of products remains largely constant between seasons in households, while for industrial activities monthly profiles are based on national electricity consumption statistics per industrial branch (e.g. manufacture of other transport equipment, wood and cork industry) and monthly motor vehicle production statistics for the specific case of the automotive industry. For industrial and domestic coating applications, a profile is proposed based on the temperature-dependent parametrization reported by Wu et al. (2024). Survey-based weekly patterns reported by Chinkin et al. (2003) for residential and commercial use of paints or solvents are considered for the development of the weekly profiles. At the hourly scale, we consider the domestic natural gas demand archetypes reported by Pullinger et al., (2024), assuming that the hourly occupancy profile associated to natural gas consumption is highly correlated with the diurnal pattern of domestic use of solvent activities. For the industrial/commercial coating applications we consider the hourly profile reported by the MapEIre project (https://projects.au.dk/mapeire/, last access: 15/06/2026). For the other industrial use of solvent categories, we assume the CAMS-REG-TEMPO profiles proposed for the manufacturing industry. For tobacco consumption, profiles are derived from cigarette sales, and tobacco consumption patterns as reported by Zhai et al. (2022).

For the road transport sector, interurban and rural monthly, weekly and hourly temporal profiles are estimated per NUTS2 region and general type of vehicle (light and heavy-duty) using measured traffic count data. At the urban scale, monthly, weekly and hourly temporal profiles are derived from TomTom congestion statistics (https://www.tomtom.com/traffic-index/, last access 15/05/2026). The TomTom congestion statistics were converted to traffic counts making use of a sigmoid equation derived from Madrid traffic counts provided by the Madrid City Council (2024) and TomTom congestion statistics for the period 2022 to 2024. Specific sigmoid equations were produced for Monday-to-Thursdays, Fridays and weekend day types (Fig. S3). The temporal profiles at the city level were averaged at the NUTS2 level considering the annual average level of congestion and number of inhabitants of each city. For evaporative emissions, the monthly and hourly profiles reported by CAMS-REG-TEMPO for Spain are considered, while a flat weekly profile is assumed.

Concerning other mobile sources and machinery (SNAP08), monthly and weekly profiles are predominantly constructed from national traffic statistics for different transport modes, including aviation and rail transport, as well as fuel consumption statistics for agricultural machinery.

Waste management (SNAP09) emissions are primarily distributed according to monthly electricity consumption statistics reported per industrial branch (e.g., wastewater collection and treatment), and hourly electricity generation data for waste-to-energy plants. For activities lacking detailed temporal information, profiles from CAMS-REG-TEMPO or flat profiles are assumed.

https://doi.org/10.5194/egusphere-2026-4146
Preprint. Discussion started: 23 July 2026

For agriculture (SNAP10), crop- and NUTS2-dependent profiles are derived from the dynamical fertilizer ammonia emission parametrization described in Guevara et al., (2020), which considers information per crop type on the fraction of fertilizer application at different stages (planting, growth and after harvest) and optimal application dates as well as meteorological parameters (temperature and wind speed). For emissions related to livestock, the monthly profiles reported by CAMS-REG-TEMPO for Spain are considered. A flat weekly profile is assumed, while the hourly temporal profile reported by CAMS-REG-TEMPO is considered.

Table 4 Summary of main proxies used for the temporal disaggregation of emissions in HERMES_Δ

Emission source	Main proxies used
SNAP01: Energy industries	- Daily electricity production reported per fuel, technology and Spanish region (Iberian Peninsula, Balearic Islands and Canary Islands) - Hourly electricity production per fuel - Monthly refinery production - Monthly coke production
SNAP02: Non-industrial combustion plants	- Fuel-dependent profiles as reported by CAMS-REG-TEMPO for Spain
SNAP03: Industrial combustion plants SNAP04: Industrial processes without combustion	- Monthly electricity consumption reported per industrial branch (e.g., chemical industry, food industry) - Monthly production statistics reported per industrial branch (i.e., cement production, iron and steel production, refinery outputs) - Weekly and hourly profiles as reported by CAMS-REG-TEMPO for Spain
SNAP05: Fugitives	- Monthly electricity consumption reported per industrial branch (e.g., coal extraction) - Monthly statistics on fossil fuel extraction, production and consumption (e.g., gasoline and diesel consumption, natural gas consumption) reported by multiple national official statistics - Hourly counts from permanent counting stations - Flat weekly and hourly profiles assumed for most of the activities due to lack of data.
SNAP06: Solvents	- For industrial use of solvent activities, monthly electricity consumption reported per industrial branch (e.g., manufacture of other transport equipment, Wood and cork industry) - Monthly motor vehicle production statistics - For coating applications, temperature-dependent monthly profiles - Survey-based weekly patterns for residential and commercial use of paints or solvents - Domestic natural gas demand archetypes , assuming that the occupancy profiles associated to natural gas consumption is highly correlated with domestic use of solvent activities - For other industrial use of solvent activities, weekly and hourly profiles as reported by CAMS-REG-TEMPO - Monthly cigarette sales and weekly and hourly tobacco consumption patterns
SNAP07: Road transport	- Hourly traffic counts from permanent stations by vehicle type (light duty and heavy duty) in interurban and rural roads - Hourly day-of-the-week dependent congestion traffic index data from TomTom for urban roads - For evaporative emissions, monthly and hourly profiles from CAMS-REG-TEMPO for Spain
SNAP08: Other mobile sources and machinery	- Monthly and weekly traffic statistics reported for multiple transport modes including aviation and rail, among others. - Monthly agricultural machinery fuel statistics
SNAP09: Waste	- Monthly electricity consumption reported per industrial branch (e.g., wastewater collection and treatment) - Hourly electricity production for waste-to-energy plants - Weekly and hourly profiles as reported by CAMS-REG-TEMPO
SNAP10: Agriculture	- Crop- and NUTS2-dependent monthly profiles for fertilizer applications - Temporal profiles derived from CAMS-REG-TEMPO for Spain for livestock and hourly profiles

https://doi.org/10.5194/egusphere-2026-4146
Preprint. Discussion started: 23 July 2026

3.1.5 Speciation profiles

For NMVOC emissions, a split into over 900 individual chemical species is performed making use of the speciation profile catalogue developed by Oliveira et al. (2026), which consists of a total 130 speciation profiles collected from the literature. The remapping of these individual NMVOC to the species of the selected gas phase chemical mechanism is performed considering the information reported by Carter (2015) for CB05, CB06 and RACM, Pye et al. (2023) for CRACMM1 and CRACMM2, and the CHIMERE wiki (https://www.lmd.polytechnique.fr/chimere/, last access: 15 May 2026) for MELCHIOR2.

The speciation split proposed for NO_x emissions assumes that 90% of total emissions are emitted as NO and 10% as NO_2 for all sectors (Houyoux et al., 2000) except for road transport, for which fuel-dependent factors are derived from NAEI (2024).

Concerning carbonaceous $PM_{2.5}$ components, HERMES_Δ considers the BC emissions reported in the official SEI inventory and estimates OC (expressed in full molecular mass) and primary sulphate considering the sector-dependent splits reported by CAMS-REG for Spain (Kuenen et al., 2022).

3.2 Emission outputs

Figure 3 and 4 present annual spatially resolved NO_x, SO_x, CO, NMVOC, NH_3, PM_{10}, $PM_{2.5}$, CH_4 and fossil fuel CO_2 emissions obtained with HERMES_Δ for Spain and the year 2023 at 0.01×0.01 deg. resolution. Results were produced for two domains, the first one covering the Peninsular Spain and Balearic Islands (Fig. 3) and the second one the Canary Islands (Fig. 4). The spatial pearson correlation coefficient (ρ) between each pollutant and fossil fuel CO_2 emissions is also provided.

Focussing on the Peninsular Spain and Balearic Islands results, it is observed how the spatial pattern can differ significantly between pollutants. NO_x is the only pollutant highly correlated with CO_2 emissions ($\rho = 0.73$), as both are primary released as byproducts of fossil fuel combustion sources, mainly including road transport and energy and manufacturing industries. The grid cells with the highest CO_2 and NO_x emissions correspond to the locations of the interurban roads with the highest AADT. The most populated cities, such as Madrid or Barcelona, as well as large industrial cluster such as the ones of Tarragona and Huelva are also clearly identifiable on the maps of these two species. Despite being also a combustion byproduct, SO_x and CO emissions present moderate correlations with CO_2 (ρ = 0.53 and 0.45, respectively). For SO_x this is because for many combustion sources (e.g., mobile sources, power plants and the majority of industrial combustion plants), the fuels consumed have a very low sulphur content (i.e., automotive gasoline/diesel fuels and natural gas) and therefore contribute a relatively small amount of SO_x when compared to CO_2. Main SO_x hotspots observed in the map correspond to specific coal- and oil-fired industrial large and small-to-medium industrial boilers in the manufacturing sector, refineries and coal- and oil-fired boilers in the commercial and residential sector, which are mainly located in the regions of Madrid, Asturias and the Basque

https://doi.org/10.5194/egusphere-2026-4146
Preprint. Discussion started: 23 July 2026

country. Anthropogenic PM_{10} emissions present a large contribution from residential and commercial biomass combustion sources, which are assumed to be carbon neutral and therefore do not report CO_2 emissions under the UNFCCC inventory, and non-combustion sources such as mining, construction activities and open field agricultural operations, and thus present a low correlation with CO_2 ($\rho = 0.3$). The spatial correlation is also low for $PM_{2.5}$ ($\rho = 0.32$) due to the carbon-neutral residential and commercial biomass combustion sources. Main PM_{10} and $PM_{2.5}$ hotspots are observed in urban areas due to the contribution of non-exhaust and exhaust road transport sources, respectively. PM emissions related to residential combustion activities are widely scattered throughout dispersed and very low-density rural areas. For PM10, large background levels are associated to agricultural land areas due to the coarse PM emissions released during harvest and land preparation operations. NMVOC and NH_3 emissions are largely linked to non-combustion sources, mainly use of solvent activities and agricultural practices (use of fertilizers and livestock management), respectively, and subsequently present a very low degree of correlation with CO_2 emissions ($\rho = 0.14$ and 0.04, respectively). Main NMVOC hotspots are linked to urban areas, where residential and commercial use of solvent activities are mapped, while NH_3 emissions are greater in regions with a higher density of livestock farms, such as Lleida and eastern Aragón. Lastly, CH_4 presents the lowest correlation with CO_2 ($\rho = 0.03$) since emissions are mainly linked to livestock and waste management.

https://doi.org/10.5194/egusphere-2026-4146
Preprint. Discussion started: 23 July 2026

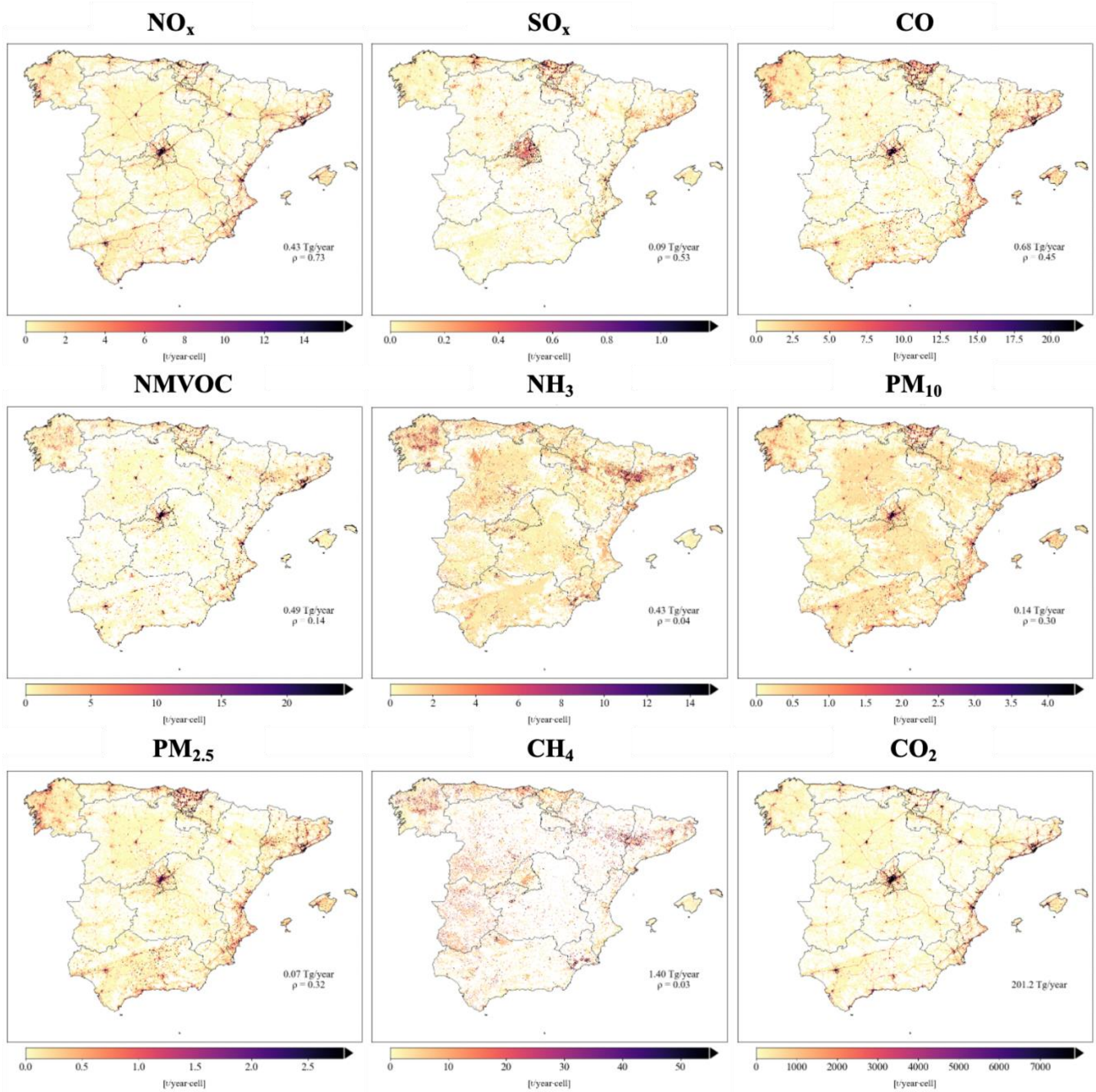

Figure 3 NO_x, SO_x, CO, NMVOC, NH_3, PM_{10}, $PM_{2.5}$, CH_4 and fossil fuel CO_2 annual gridded emissions maps at 0.01×0.01 deg [$t \cdot year^{-1} \cdot cell^{-1}$] for the year 2023 for Peninsular Spain and Balearic Islands. Total annual emissions [$Tg \cdot year^{-1}$] and spatial Pearson correlation coefficient (ρ) between each species and CO_2 is shown in the bottom right of each map.

https://doi.org/10.5194/egusphere-2026-4146
Preprint. Discussion started: 23 July 2026

For the Canary Islands, SO_x, $PM_{2.5}$ and PM_{10} are the pollutants that present the largest correlations with CO_2 emissions (ρ = 0.68, 0.67, 0.6, respectively), while for NO_x (CO) the correlation is a bit lower (higher) than the one showed for the Iberian Peninsula domain (ρ = 0.57 and 0.58). We believe the discrepancies between the two domains are mainly driven by the following two factors: i) emissions from the Canary Island oil-fired power plants dominate the majority of SO_x emissions (more than 95%) and almost half of the CO_2 emissions and ii) the use of biomass in the commercial and residential sector for heating purposes is very residual due to climatological conditions, which entails that a large part of PM emissions are related to the aforementioned power plants (close to 30%) and road transport emissions (also close to 30%), the later representing almost 40% of total CO_2 emissions. Low degree of correlation is observed for NMVOC (0.11), NH_3 (0.02) and CH_4 (0.01) in line with the results reported for the Iberian Peninsula domain.

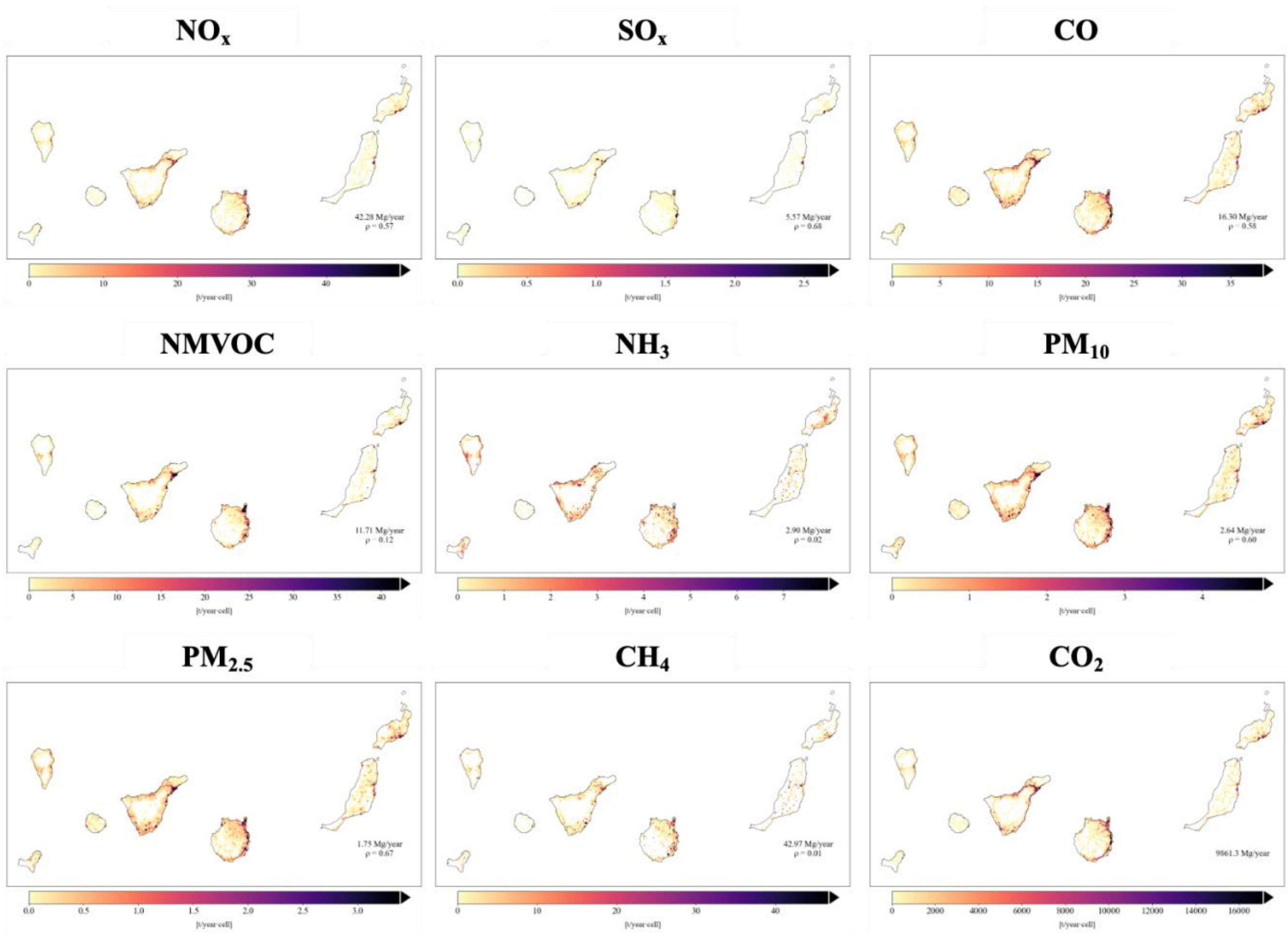

Figure 4 Same as Fig.3 but for the Canary Islands.

https://doi.org/10.5194/egusphere-2026-4146
Preprint. Discussion started: 23 July 2026

Figure 5 and 6 show the gridded annual NO_x and $PM_{2.5}$ emissions at 0.01×0.01 deg resolution produced by HERMES_Δ for the year 2023 over three selected urban metropolitan regions, including Asturias (NW of Spain), Barcelona (NE of Spain) and Palma de Mallorca (Balearic Islands). Monthly, weekly and diurnal emission temporal distributions per sector are also provided for each metropolitan region and pollutant. The three selected regions represent different sociodemographic and climatological conditions, which are both reflect in the proxies considered in HERMES_Δ and corresponding results.

NO_x emissions in Asturias are dominated by the public power and industrial combustion sectors (71%), while in Barcelona emissions are dominated by the road transport and industrial combustion sectors (70%) and in Palma de Mallorca by road and non-road transport activities, mainly air traffic in the Palma–Son Sant Joan airport (76%). Asturias and Barcelona present a rather flat seasonality, with emissions slightly decreasing in Barcelona during January and August due to a decrease in urban road transport emissions. A more pronounced seasonality is observed in Palma de Mallorca due to the influence of tourism, with road, non-road transport and public power emissions increasing more than 60% during summer months when compared to winter. Despite being dominated by different sectors, similar weekly profiles are reported in each metropolitan regions, with emissions being almost constant during working days and dropping between weekdays and weekends by approximately 23%. The drop is mainly linked to a drop in road transport emissions in all three cases. At the hourly scale, Asturias shows a rather flat distribution of total emissions, resulting in a smaller contrast between nigh-time (23:00 to 06:00 h LT) and daytime (07:00 to 22:00 h LT) total NO_x emissions (-29% reduction between night- and daytime) when compared to Barcelona and Palma de Mallorca (-44% reduction). This result is driven by the differences between hourly profiles proposed for the public power and manufacturing industry sectors and the ones proposed for the road transport and air traffic activities, the later showing a more pronounced change between daytime and nighttime, when number of circulating cars and airplanes significantly decreases. Most of the NO_x hotspots reported in Asturias correspond to specific energy and manufacturing industries (isolated grid cells), whereas in the case of Barcelona and Palma de Mallorca these correspond to the roads providing access to the city centres and the airports located south-west and east, respectively.

$PM_{2.5}$ emissions in Asturias are largely dominated by industrial processes (48%), while Barcelona and Palma de Mallorca present two dominant sectors each: industrial combustion and road transport (36% and 29%) and non-industrial combustion and road transport (42% and 27%), respectively. For Barcelona, it is important to note the contribution from solvents and other products (11%), which is mainly linked to tobacco consumption. The seasonality in Asturias and Palma de Mallorca is very different to the one reported for NO_x, with emissions showing a drop during summer due to the reduction of non-industrial combustion activities, mainly driven by space heating needs. The contrast between winter and summer time is especially large in Palma de Mallorca, where $PM_{2.5}$ emissions decrease by 42%. A near-flat monthly distribution is observed in Barcelona, like the one reported for NO_x. A drop between weekdays and weekends is observed in Asturias and Barcelona, in line with what has previously discussed for NO_x. In the case of Palma de Mallorca, emissions remain almost constant during the whole week, with a slight increase being observed on Fridays. This result is a combination of two factors; i) non-industrial combustion

https://doi.org/10.5194/egusphere-2026-4146
Preprint. Discussion started: 23 July 2026

emissions are assumed to increase during Friday and the weekend, as residential biomass combustion activities are associated to recreational purposes and ii) road transport activities significantly decrease during the weekend, compensating the aforementioned increase. Large discrepancies are observed between the hourly distributions of $PM_{2.5}$ reported in the three selected regions. Palma de Mallorca reports much higher emissions during the evening hours (17:00–22:00 h LT) mainly due to the hourly distribution of non-industrial combustion emissions, which are largely linked to residential biomass combustion activities in fireplaces and are assumed to peak in the evening. In contrast, in Asturias emissions are distributed more evenly during the day, with differences between daytime and nighttime being much lower due to the near-flat distribution assumed for industrial processes emissions. The $PM_{2.5}$ hourly distribution in Barcelona is similar to the one estimated for NO_x, with the contrast between daytime and nighttime being slightly lower due to the larger contribution of industrial combustion emissions, that present a near-flat diurnal distribution. In terms of spatial mapping, main hotspots in Asturias are related to industrialised land use areas and specific grid cells where large point sources are located. Similarly, in Barcelona the largest hotspots are linked to industrialised areas. Finally, in Palma de Mallorca large hotspots are observed in suburbs and rural areas linked to non-industrial combustion emissions.

https://doi.org/10.5194/egusphere-2026-4146
Preprint. Discussion started: 23 July 2026

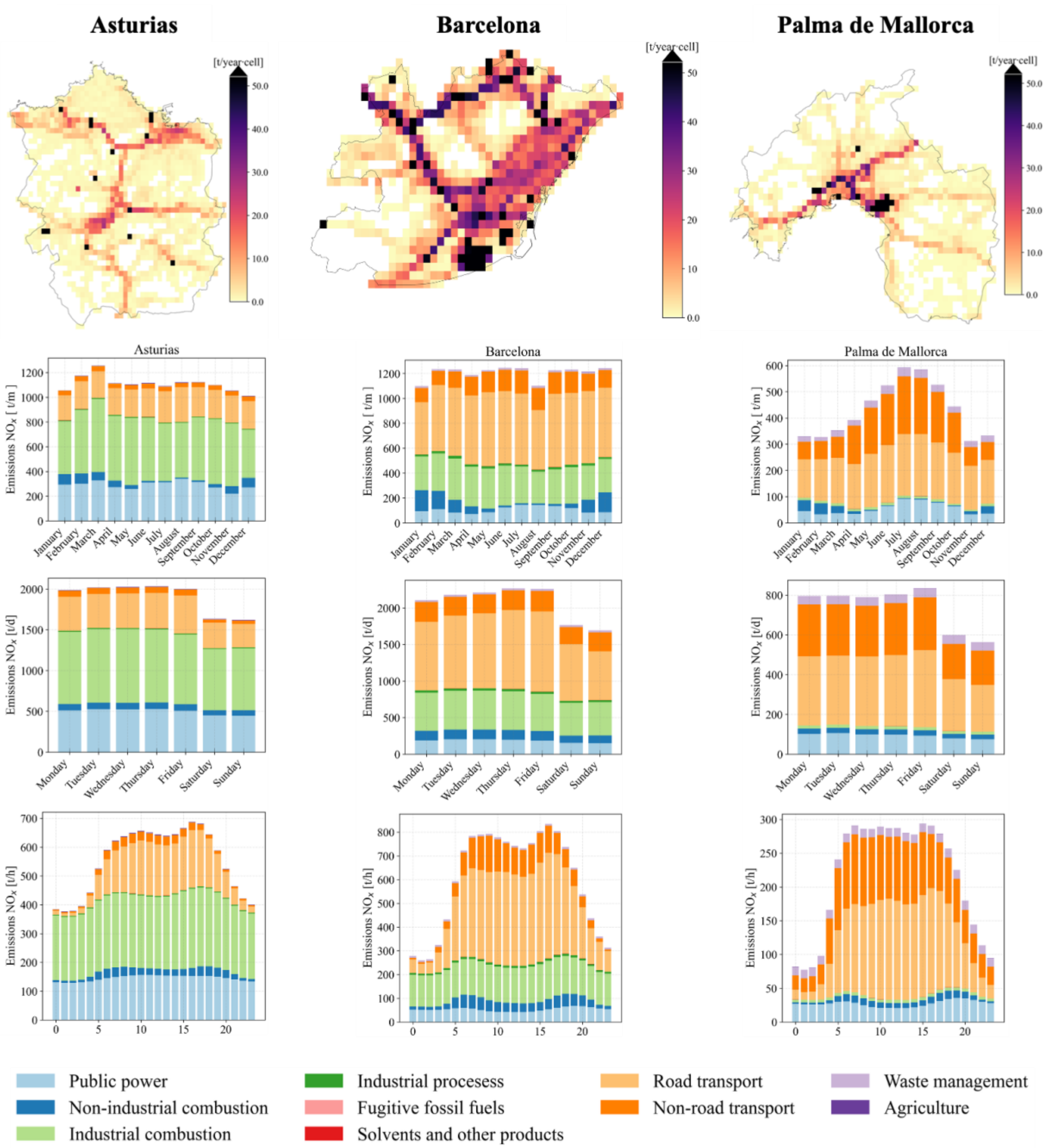

Figure 5 Gridded annual NO_x emissions (0.01×0.01 deg; t·year^{-1}·cell^{-1}) and monthly, weekly and diurnal emission temporal distributions per sector produced by HERMES_Δ for the year 2023 over the urban metropolitan regions of Asturias (NW of Spain), Barcelona (NE of Spain) and Palma de Mallorca (Balearic Islands).

https://doi.org/10.5194/egusphere-2026-4146
Preprint. Discussion started: 23 July 2026

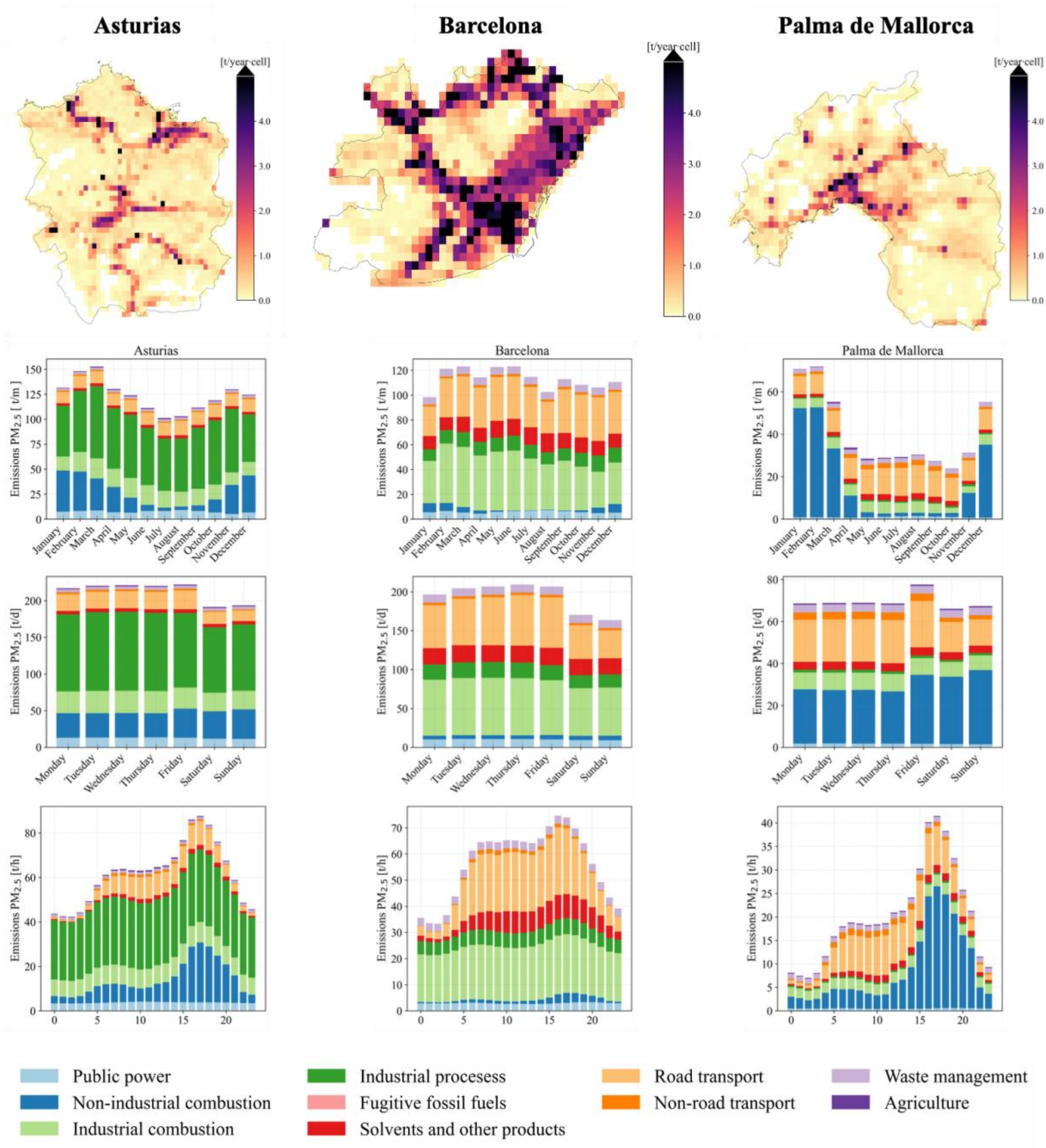

Figure 6 Same as Fig. 5 but for $PM_{2.5}$

Figure 7 shows examples of the portions of the speciated CB05 and CRACMM1 species of total annual NMVOC estimated by HERMES_Δ for Spain (Peninsular Spain and Balearic Islands) and the metropolitan area of Madrid.

https://doi.org/10.5194/egusphere-2026-4146
Preprint. Discussion started: 23 July 2026

Concerning the CB05 speciated results, the PAR species (paraffin carbon bonds) is by large the most abundant in both domains (76.3% and 83.5% of total NMVOC). This is because PAR is a lumped model species that represent all singly bonded carbon compounds, including alkanes (e.g., propane, butane), ketones (specifically acetone) and other compounds and fragments from larger oxidized molecules (Yarwood, 2005). The strategy behind the CB05 chemical mechanism, which was developed at the beginning of the 2000s when high-performance computing was less advanced, is to find a compromise between computational load and realistic simulation of secondary pollutants. ETOH (ethanol) and ETH (ethene) are the second and third most abundant CB05 species emitted both at the national level and for the area of Madrid, with contributions raging between 7.8 and 9.7% and 2.1 and 4.1%, respectively.

The speciated results produced for the CRACMM1 chemical mechanism, which was released only 3 years ago, present a wider range of dominant model species. This is because CRACMM1 aggregates NMVOC emissions by molecule based on their functional groups, number of carbons, reactivity with OH radicals and volatility, thus incorporating a more comprehensive set of species when compared to CB05 (Pye et al., 2023). For example, instead of assigning all alkanes under a single lumped species, 3 classes of alkane-like species are considered, including HC3 (C3 alkanes), HC5 (C5 alkanes) and HC10 (C8 or more alkanes). EOH (ethanol) and HC3 are the two dominant species at the national level (21.8% and 16.2%), followed by ETE (ethene), HC5, ACT (acetone) and ORA2 (acetic acid and higher acids), all of them presenting contributions between 10 and 5%. In the metropolitan region of Madrid, HC3, EOH and ACT represent together more than 60% of total NMVOC. Compared to the national level, relative contributions from HC3 and ACT are almost two times larger (32.1% and 9.8%). This is mainly attributed to the large contributions of road transport and solvent use to total NMVOC emissions in urban areas, in particular of n-butane, ethyl acetate and propane from road transport and of acetone from the domestic use of solvents.

https://doi.org/10.5194/egusphere-2026-4146
Preprint. Discussion started: 23 July 2026

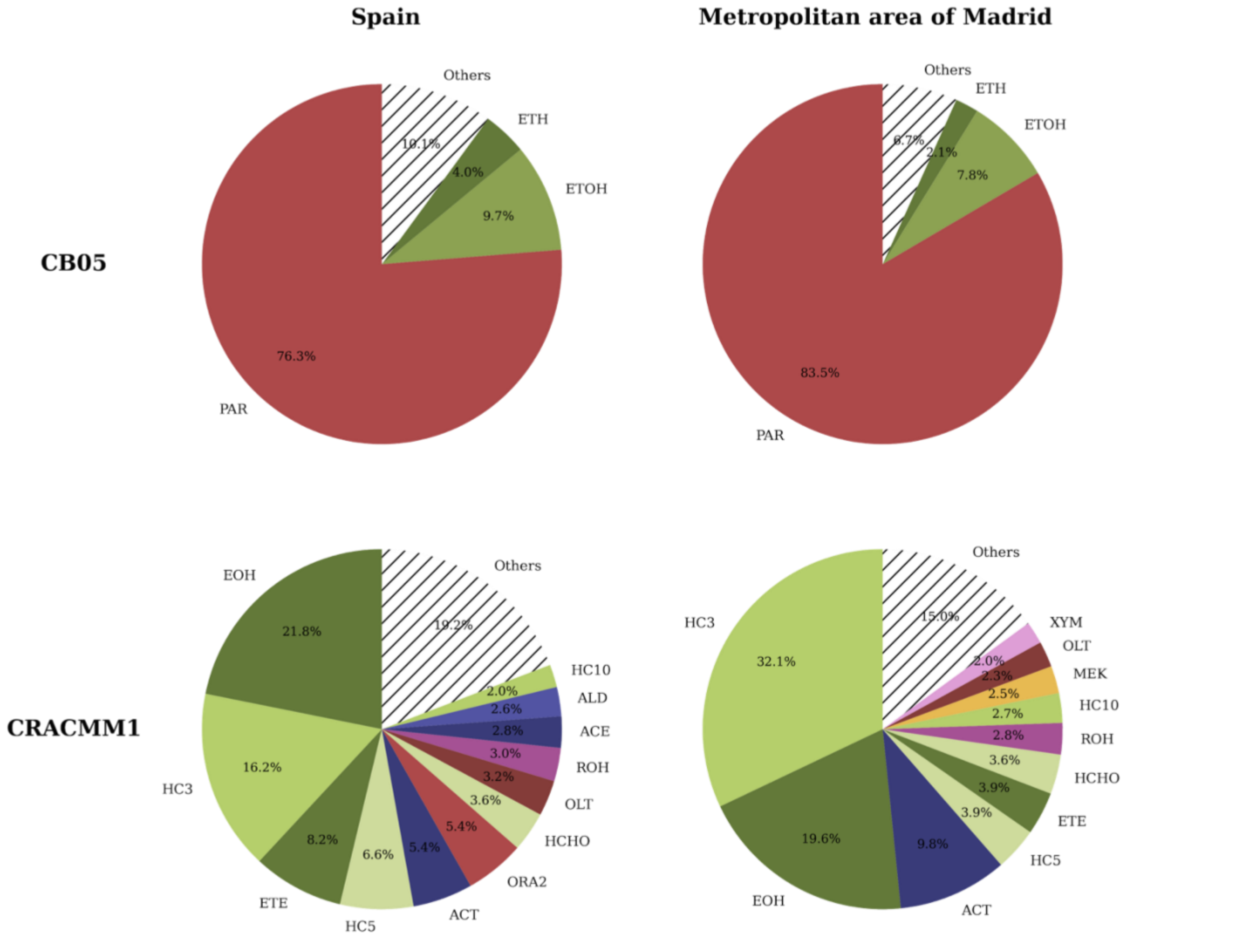

Figure 7 Composition (in %) of total annual NMVOC emissions according to the speciated model species considered by the CB05 and CRACMM1 chemical mechanisms. Results are provided for Spain and the metropolitan area of Madrid. All the individual chemical species with a share lower than 2% are grouped under the "Others" category.

3.3 Computational performance

This section evaluates the computational performance of HERMES_Δ through a representative benchmark experiment. The analysis focuses on two complementary aspects of the model execution: (i) the computational cost associated with the generation of the auxiliary files required for the spatial mapping of emissions, and (ii) the parallel scalability of the emission processing workflow with increasing number of MPI processes.

The benchmark experiment is defined over the same Peninsular Spain and Balearic Islands gridded domain at 0.01° × 0.01° resolution considered in Sect. 3.2. The domain extends from 34.0°N to 44.5°N and from 10.0°W to 4.5°E, resulting in a grid composed of 1050 × 1450 horizontal cells and 24 vertical layers. This corresponds to approximately 1.52 million horizontal

https://doi.org/10.5194/egusphere-2026-4146
Preprint. Discussion started: 23 July 2026

grid cells and 36.5 million three-dimensional grid cells. The emissions used in the experiment correspond to the 10 SNAP sectors (SNAP01–SNAP10). For the chemical speciation step, the CB05+AERO5 chemical mechanisms are selected, which implies splitting the original inventory air pollutants (NO_x, SO_x, NMVOC, CO, NH_3, PM_{10}, $PM_{2.5}$ and BC) into a total of 38 output chemical species. All experiments were executed on the Marenostrum 5 supercomputer, hosted by the BSC, using the General Purpose Partition (GPP) and MPI parallelization.

Based on this configuration, two complementary analyses are performed in the following subsections. Section 3.3.1 evaluates the computational cost associated with the creation of the auxiliary files required during the initialization stage of HERMES_Δ, whereas Section 3.3.2 analyses analyzes the parallel scalability of the emission processing workflow by measuring execution time, speed-up, and parallel efficiency across different numbers of MPI processes.

3.3.1 Creation of auxiliary files for the spatial mapping

During the initialization stage, HERMES_Δ generates several auxiliary files required for the spatial mapping of emissions. These auxiliary datasets include, among others, the normalization of spatial proxies, the mapping between emission sources and the target grid and additional preprocessing steps required to efficiently perform the emission calculations during the simulation. As previously indicated, these auxiliary files are stored in NetCDF format after their creation so that they can be reused in subsequent executions that consider the same working domain.

The computational cost associated with this preprocessing stage depends on the characteristics of the emission sector being processed. In particular, different SNAP sectors rely on different types of spatial proxies (see Sect. 3.1.2), which can involve vector geometries, point sources, or high-resolution raster datasets. As a consequence, the initialization cost can vary significantly between SNAP sectors.

To quantify this cost, the auxiliary file generation time was evaluated independently for each of the 10 SNAP sectors. For sectors SNAP01 to SNAP09, the preprocessing workflow was executed using 32 MPI processes. The SNAP10 sector requires substantially larger computational resources due to the use of the EUCROPMAP proxy (10 m spatial resolution). For this reason, the preprocessing workflow for SNAP10 was executed using 256 MPI processes.

For each sector, two types of executions were performed. In the first execution, the model generates the auxiliary files required by the sector (“create” mode). In the second execution, the previously generated auxiliary files are reused (“read” mode). Both executions still perform additional initialization tasks required by the model, such as the preparation of chemical speciation profiles and the configuration of temporal and vertical distribution parameters. To reduce the impact of runtime variability

https://doi.org/10.5194/egusphere-2026-4146
Preprint. Discussion started: 23 July 2026

inherent to HPC environments, each experiment was repeated five times, and the reported values correspond to the average mean execution time across these replications.

Table 5 summarizes the execution times required to generate and read the auxiliary files for each SNAP sector. The results show that the initialization time is strongly dependent on the spatial proxies used by each sector. Sectors relying on relatively simple spatial inputs (i.e., point source proxies reported as GeoJSON files) exhibit relatively small differences between the "create" and "read" executions, whereas sectors involving more complex spatial preprocessing show substantially larger initialization costs. In particular, sectors such as SNAP02, SNAP07, and SNAP08 present significant preprocessing overheads due to the spatial operations required to generate the auxiliary datasets, which involve the processing of high-resolution population density rasters and large polyline shapefiles (see Sect. 3.1.2). The most computationally demanding case corresponds to SNAP10, which relies on the 10m high-resolution EUROCROPMAP and therefore requires more intensive spatial processing.

Overall, the results highlight that the generation of auxiliary files can represent a substantial portion of the initialization time during the first execution of the model. However, once these auxiliary datasets are created, they can be reused in subsequent simulations, significantly reducing the initialization cost and enabling more efficient repeated executions of HERMES_Δ for the same spatial configuration.

Table 5 Mean execution time (in seconds) required to generate and read the auxiliary files during the initialization stage of HERMES_Δ for each SNAP sector. The "Create" column corresponds to the execution where the auxiliary files are generated, while the "Read" column corresponds to executions where previously generated auxiliary files are reused. The "Difference" column represents the additional computational cost associated with generating the auxiliary files. Values correspond to the average of five independent executions.

Sector	Create (s)	Read (s)	Difference (s)
SNAP01	55.84	21.84	34.00
SNAP02	365.75	19.66	346.09
SNAP03	55.51	25.42	30.09
SNAP04	177.02	34.65	142.37
SNAP05	79.38	20.49	58.88
SNAP06	201.53	27.12	174.41
SNAP07	387.75	18.84	368.92
SNAP08	240.40	19.19	221.21
SNAP09	164.05	21.32	142.72
SNAP10	1548.44	41.86	1506.59

https://doi.org/10.5194/egusphere-2026-4146
Preprint. Discussion started: 23 July 2026

3.3.2 Scalability analysis

The parallel scalability of HERMES_Δ was evaluated by executing the full emission processing workflow using different numbers of MPI processes, ranging from 1 to 32. All experiments were performed under the same configuration described in the previous subsection, ensuring that only the degree of parallelism varied between runs. Previously generated auxiliary files were reused during all scalability experiments (i.e., no auxiliary files were created during the benchmark), NetCDF compression was disabled and all executions were performed on a single MareNostrum5 compute node using between 1 and 32 MPI processes.

To ensure statistical robustness, each configuration was executed 10 times. The reported execution times correspond to aggregated values obtained after applying an outlier detection procedure. Specifically, outliers were identified using the interquartile range (IQR) method with a threshold of 1.5, and only inlier values were retained. The mean of the remaining values was taken to obtain a representative execution time for each configuration. This approach reduces the impact of transient variability in the HPC environment.

Figure 8 shows the total execution time as a function of the number of MPI processes, together with the contribution of the main processing components: initialization, spatial allocation of point sources (PointSourcesAllocation), speciation, vertical distribution (vertical), temporal distribution (temporal), horizontal distribution (horizontal) and write, while Table 6 summarizes the corresponding total execution time, speed-up and parallel efficiency A substantial reduction in execution time is observed when increasing the number of processes from 1 to 4, moving from 92.5 to 29.4 minutes and indicating effective parallelization of part of the workflow. However, beyond 8 processes, the reduction in runtime becomes progressively smaller, and the curve tends to flatten, showing an execution time reduction of less than 8.2 minutes when moving from 8 to 32 processes. Most of the computational work is done during the horizontal mapping (between 85.1% and 32.5 %), followed by the initialization process and the writing of the emission output file, which increasingly become the main time consumers when increasing the number of processes (up to 28.4% and 35.5% of the total time when using 32 processes).

This behaviour is explained by the heterogeneous scalability of the different components. While some exhibit good parallel performance, others remain largely insensitive to the number of processes, thus limiting the overall speed-up. The horizontal distribution module, which is the computational core of the model, exhibits near-ideal scalability, which confirms that it is well suited for parallel execution. In contrast, other steps including speciation, vertical distribution, and temporal allocation, show limited or negligible speed-up, indicating that these stages are either not parallelized or dominated by overheads. The writing stage exhibits sub-linear and even negative scaling, suggesting the presence of I/O bottlenecks or contention effects when increasing the number of processes. An illustration of the speed-up achieved by the model is shown in Fig. S6.

https://doi.org/10.5194/egusphere-2026-4146
Preprint. Discussion started: 23 July 2026

From a practical perspective, the optimal configuration for the tested setup is found between 8 and 16 MPI processes, where a balance between execution time reduction and resource efficiency is achieved.

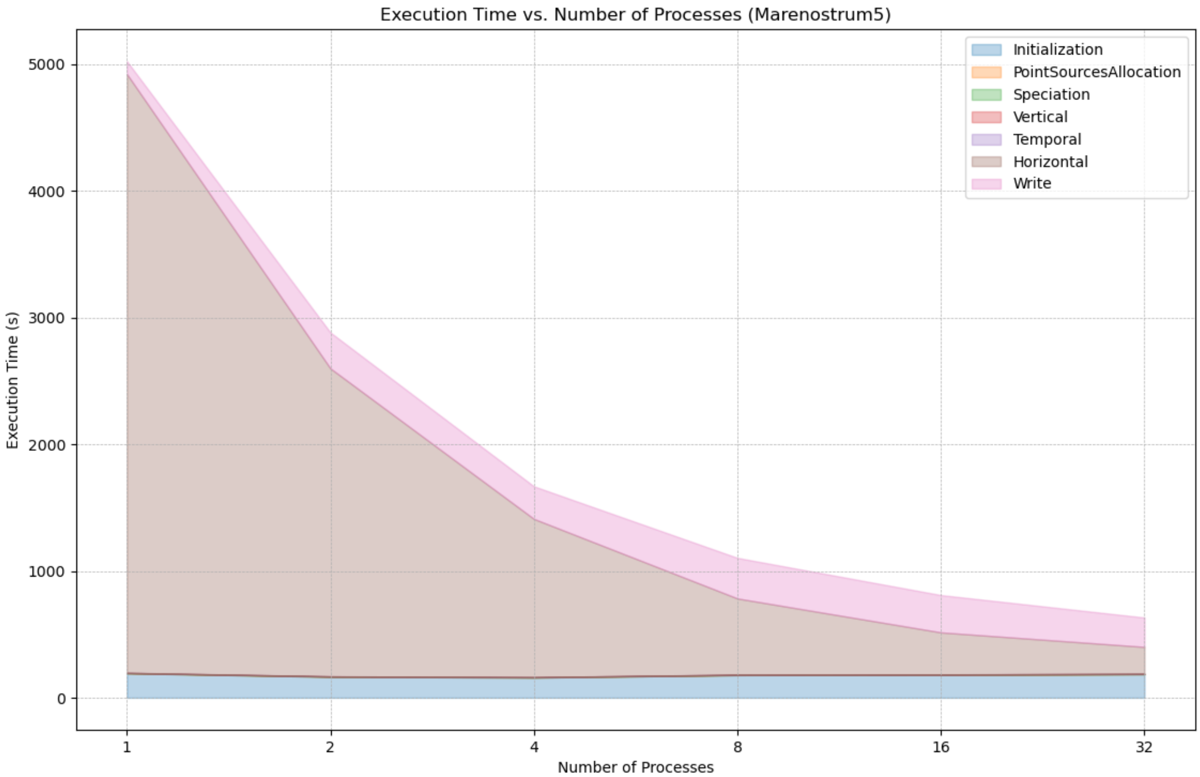

Figure 8 Total execution time as a function of the number of MPI processes for the HERMES_Δ workflow executed on MareNostrum5. The stacked areas represent the contribution of the main processing components, including initialization, point sources allocation, speciation, vertical distribution, temporal allocation, horizontal mapping, and output writing. The results correspond to the mean values obtained from 10 independent replications after outlier filtering using the interquartile range (IQR) method (threshold = 1.5). The figure highlights the reduction in execution time with increasing parallelism, as well as the relative contribution of each component to the total computational cost

Table 6 Total execution time, speed-up and parallel efficiency of the complete HERMES_Δ workflow executed on MareNostrum5 using different numbers of MPI processes. Speed-up is computed with respect to the single-process execution, and parallel efficiency is defined as the speed-up divided by the number of MPI processes.

MPI processes	Total execution time (s)	Speed-up	Parallel efficiency
1	5550.62	1.00	100.00
2	3086.33	1.80	89.92
4	1763.44	3.15	78.69
8	1143.32	4.85	60.69
16	833.93	6.66	41.60
32	653.33	8.50	26.55

https://doi.org/10.5194/egusphere-2026-4146
Preprint. Discussion started: 23 July 2026

4 Conclusions

This paper presents the HERMES_Δ software, an open-source, Python-based, parallel and flexible emission system that processes official inventories of air pollutants (NO_x, SO_x, CO, NH_3, NMVOC, PM_{10}, $PM_{2.5}$ and BC) and GHG (CO_2 and CH_4) from anthropogenic sources to adapt them in a flexible and transparent way for use in 3D atmospheric transport and chemistry models. Original emissions at source sector and industrial facility-level are processed applying a detailed horizontal, vertical, temporal and chemical speciation treatment to produce ready-to-use modelling emissions compatible with multiple user-defined grids, chemical mechanisms and 3D mesoscale modelling systems. HERMES_Δ allows integrating and processing multiple European, national and subnational proxies, statistics and speciation profiles to accurately reflect key spatio-temporal and speciation aspects of anthropogenic emissions. Another advantage of HERMES_Δ is that it provides self-consistent air pollutants and GHG emissions, thus enhancing the integrated analysis of emissions affecting both air pollution and climate change.

We exemplify the use of HERMES_Δ by processing the Spanish national emission inventory making use of a catalogue of more than 2500 official point sources provided at their exact geographical location and a total of 140 spatial proxies, more than 660 monthly, weekly and hourly temporal profiles and 130 sector-dependent chemical speciation profiles. Examples of spatially and temporally resolved as well as speciated emission outputs for Spain are provided and discussed to illustrate the capabilities of HERMES_Δ, together with an evaluation of its computational performance.

HERMES_Δ is currently being implemented within the MOCAGE chemical transport model (Josse et al., 2004) as part of the Spanish national air quality forecasting system developed and maintained by the Spanish Meteorological Agency (https://www.aemet.es/en/eltiempo/prediccion/calidad_del_aire?opc1=calidad, last access 01/06/2026) as well as within the MONARCH chemical transport model (Badia et al., 2017) as part of the CALIOPE regional air quality forecasting system developed and maintained by the BSC (https://caliope.bsc.es/, last access 01/06/2026). Besides these two on-going implementations, HERMES_Δ is also currently used to perform simulation of CO_2 concentrations in the metropolitan area of Barcelona and to understand the role of anthropogenic versus biogenic sources using the WRF-Chem GHG system (Luo et al., 2026). The high-resolution emissions produced by HERMES_Δ can support not only modelling applications in line with the European AAQD and current GHG monitoring efforts, but also artificial intelligence driven and proxy-based downscaling strategies to downscale air quality modelling results to higher resolutions (e.g., d'Hondt and Petetin, 2026).

https://doi.org/10.5194/egusphere-2026-4146
Preprint. Discussion started: 23 July 2026

4.1 Applicability to other countries

HERMES_Δ is generic and flexible tool designed so that it can be applicable to any European countries. To this end, flexibility in input data formats and content is given by: i) allowing the user to choose the emission category nomenclature (e.g., NFR, SNAP or an arbitrary classification) and spatial aggregation level (e.g., NUTS1, 2 or 3) at which original emissions are provided to the model and ii) accepting multiple formats of georeferenced spatial proxies (GeoJSON, shapefiles, raster files). HERMES_Δ also provides flexibility in the definition of the gridded working domain, format of the output emission files and selection of chemical mechanisms. The model has been developed with a generic vision and following the same principles of flexibility and transparency as the ones considered in other versions of the HERMES software, which have successfully been implemented in other countries and in the framework of other modelling chains (e.g., Piccoli et al., 2024; Seeman et al., 2024). The main inputs required to run HERMES_Δ include official emission inventories, spatial proxies, and temporal, vertical and speciation profiles. While information on official emission inventories is granted in all Member States due to the reporting and transparency obligations associated to the CLRTAP, NECD and UNFCCC, accessibility and availability to the proxies and profiles needed to process these inventories may vary from country to country and subsequently limit the usability of the tool in certain regions. To overcome this limitation, the Spanish use case described in the paper, and particularly the detailed description of input datasets, statistics and methods considered to construct the proxies and profiles, can be regarded as a guidance for potential applications in other countries. In this sense, it is important to note that several of the proposed proxies and profiles are not specific for Spain, but have a European coverage, which means that they can be also applied for other countries. These include the EUROCROPMAP, CLC, GHSL and OSM spatial proxies, the CAMS-REG-TEMPO temporal profile dataset, and the European NMVOC speciation profile database proposed by Oliveira et al. (2026).

4.2 Future perspective

There are a series of limitations that have already been identified and that we plan to address in future versions of the model, including:

- Street scale resolution: HERMES_Δ can produce emissions with flexible spatial resolutions and for several map projections. While the model can cover the highest resolution at which 3D mesoscale models typically run (i.e., 1km × 1km), the current emission outputs do not fulfil the spatial input requirements of street-scale air pollution models that need to be used to properly capture the representation of air pollutants in high dense and complex urban environments (e.g., Benavides et al., 2019).
- Vertical allocation of point source emissions: In its current version, HERMES_Δ propose a static vertical allocation of industrial emissions based on a combination of stack height information and a fix plume rise factors defined by the user for each individual industrial facility. However, many studies have shown that large day-to-day variations of point sources' effective emission heights can occur due to changes in the meteorological parameters and atmospheric stability driving the plume rise (e.g., Guevara et al., 2024). This limitation will be fixed in future versions of the code

by explicitly using a plume rise model that considers stack and meteorological parameters as described in Guevara et al. (2020).

- Missing sources: There are emissions sources that are currently not included in official emission inventories but that can present relevant contributions to air pollution levels, especially in urban areas, mainly: road dust resuspension (e.g., Rodríguez-Rey et al., 2021) and residential and commercial cooking emissions (e.g. Ots et al., 2016). Future works will assess how to develop bottom-up annual estimates of these emissions sources an integrate them into HERMES_Δ to process them together with the official reported sources.
- Computational performance: Although the computational core of the model exhibits excellent scalability, the overall performance is slightly constrained by initialization overhead and I/O operations. Further improvements in scalability will focus on addressing the identified bottlenecks, particularly by parallelizing the initialization phase and optimizing the I/O strategy.

Future works will also focus on performing a full evaluation of the model-ready emission data obtained with HERMES_Δ for Spain through direct comparisons with other existing bottom-up and satellite-based inventories, and, on the other hand, by using it as input to the in-house MONARCH chemical transport model. We expect that the results obtained from these evaluation works will allow identifying opportunities from improvement concerning the functionalities implemented in HERMES_Δ for the spatiotemporal and speciation treatment of the original emission inventories.

5 Code and data availability

The HERMES_Δ code package (version 1.0.1) is provided through a Zenodo repository (https://doi.org/10.5281/zenodo.21393948; Tena et al., 2026a). The software is maintained as a Github repository hosted at https://github.com/BSC-ES/HERMES_Delta (last access: 15/05/2026). A wiki of the model with instructions on how to install and run it, a detailed description of the configuration and input files, and a benchmark case is also included in the Github repository. A benchmark case is provided through a Zenodo repository (https://doi.org/10.5281/zenodo.21471814; Tena et al., 2026b), including input and output files as well as the necessary scripts and instructions on how to run it, and should be used as a guideline concerning the format and content that input files provided by the users must follow. The HERMES_Δ code and the benchmark case are licensed under GNU General Public License (GPL) version 3 (GPLv3: https://www.gnu.org/licenses/gpl-3.0.ca.html, last access: 15/05/2026) and CC BY 4.0 (https://creativecommons.org/licenses/by/4.0/, last access: 20/07/2026), respectively. Bug reports and other issues should be posted to the issue tracker at https://github.com/BSC-ES/HERMES_Delta/issues (last access: 15/05/2026). All the information sources and corresponding references used to produce the HERMES_Δ input database for the Spanish use case are provided in the Supplementary material. Access to this input database can be requested upon reasonable request to the corresponding author, subject to approval.

https://doi.org/10.5194/egusphere-2026-4146
Preprint. Discussion started: 23 July 2026

6 Author contribution

MG conceived and coordinated the scientific development of HERMES_Δ. CT coordinated the technical development of HERMES_Δ's code. PC, AA and KO were responsible for the preparation of HERMES_Δ's input data for the Spanish case and performed the HERMES_Δ run cases presented in the paper. CP, JG and LR contributed to the development of HERMES_Δ's code and to the experiments to test the performance of the parallel implementation. All co-authors contributed to the testing and the documentation (wiki) of HERMES_Δ and the writing of the manuscript. MG prepared the paper with contributions from all co-authors.

7 Competing interests

The authors declare that they have no conflict of interest.

8 Acknowledgements

The present work was funded through the RESPIRE project, which is part of the Recovery, Transformation and Resilience Plan (Plan de Recuperación, Transformación Resiliencia, PRTyR) funded by the European Commission to repair the harm caused by the Covid-19 crisis, and the I+D+i project PCI2024-155065-2 funded by MICIU/AEI/10.13039/501100011033 and by the European Union. The authors would like to acknowledge J. Pérez-Ilzarbe, C. Ramos and the Spanish National Emission Inventory team from MITECO for the information provided on the emission inventory and their feedback on the analysis of the results. We also thank the support of the Generalitat de Catalunya Department of Research and Universities to the Atmospheric Composition Research Group (Code: 2021 SGR 01550). The authors acknowledge Red Española de Supercomputación (AECT-2024-2-0012, AECT-2024-3-0001) and EuroHPC JU (project ID EHPC-EXT-2025E01-095) for awarding access to MareNostrum5 and technical support. Paula Castesana acknowledges her AI4S fellowship within the "Generación D" initiative by Red.es, Ministerio para la Transformación Digital y de la Función Pública, for talent attraction (C005/24-ED CV1), funded by NextGenerationEU through PRTR.

9 References

Axelrod, K. M., Gordon, M., Koushafar, M., Hao, J., Makar, P. A., Fathi, S., and Sohn, G.: Evaluation of plume rise parameterizations in GEM-MACHv2 with analysis of image data using a deep convolutional neural network, EGUsphere [preprint], https://doi.org/10.5194/egusphere-2025-4582, 2025.

Badia, A., Jorba, O., Voulgarakis, A., Dabdub, D., Pérez García-Pando, C., Hilboll, A., Gonçalves, M., and Janjic, Z.: Description and evaluation of the Multiscale Online Nonhydrostatic AtmospheRe CHemistry model (NMMB-MONARCH)

https://doi.org/10.5194/egusphere-2026-4146
Preprint. Discussion started: 23 July 2026

version 1.0: gas-phase chemistry at global scale, Geosci. Model Dev., 10, 609–638, https://doi.org/10.5194/gmd-10-609-2017, 2017.

Baldasano, J. M., Guereca, L. P., Lopez, E., Gasso, S., and Jimenez-Guerrero, P.: Development of a high-resolution (1 km x 1 km, 1 h) emission model for Spain: The high-elective resolution modelling emission system (HERMES), Atmos. Environ., 42, 7215–7233, https://doi.org/10.1016/j.atmosenv.2008.07.026, 2008.

Balsamo, G., Engelen, R., Thiemert, D., Agusti-Panareda, A., Bousserez, N., Broquet, G., Brunner, D., Buchwitz, M., Chevallier, F., Choulga, M., Denier Van Der Gon, H., Florentie, L., Haussaire, J.-M., Janssens-Maenhout, G., Jones, M. W., Kaminski, T., Krol, M., Le Quéré, C., Marshall, J., McNorton, J., Prunet, P., Reuter, M., Peters, W., and Scholze, M.: The CO2 Human Emissions (CHE) Project: First Steps Towards a European Operational Capacity to Monitor Anthropogenic CO2 Emissions, Front. Remote Sens., 2, 707247, https://doi.org/10.3389/frsen.2021.707247, 2021.

Belda, M., Benešová, N., Resler, J., Huszár, P., Vlček, O., Krč, P., Karlický, J., Juruš, P., and Eben, K.: FUME 2.0 – Flexible Universal processor for Modeling Emissions, Geosci. Model Dev., 17, 3867–3878, https://doi.org/10.5194/gmd-17-3867-2024, 2024.

Bieser, J., Aulinger, A., Matthias, V., Quante, M., and Builtjes, P.: SMOKE for Europe – adaptation, modification and evaluation of a comprehensive emission model for Europe, Geosci. Model Dev., 4, 47–68, https://doi.org/10.5194/gmd-4-47-2011, 2011.

Binkowski, F. S., and Roselle, S.J.: Models-3 Community Multiscale Air Quality (CMAQ) model aerosol component 1. Model description, J. Geophys. Res., 108, 4183, doi:10.1029/2001JD001409, D6, 2003.

Borge, R., Lumbreras, J. and Rodríguez, E.: Development of a high-resolution emission inventory for Spain using the SMOKE modelling system: A case study for the years 2000 and 2010, Environmental Modelling & Software, 23, 1026-1044, https://doi.org/10.1016/j.envsoft.2007.11.002, 2008.

Carter, W. P. Development of a database for chemical mechanism assignments for volatile organic emissions. Journal of the Air & Waste Management Association, 65, 1171–1184, https://www.tandfonline.com/doi/abs/10.1080/39310962247.2015.1013646, 2015.

Chinkin, L.R., Coe, D.L., Funk, T.H., Hafner, H.R., Roberts, P.T., Ryan, P.A., Lawson, D.R.: Weekday versus Weekend Activity Patterns for Ozone Precursor Emissions in California's South Coast Air Basin, Journal of the Air & Waste Management Association, 53:7, 829-843, DOI: 10.1080/10473289.2003.10466223, 2003.

Colette, A., Collin, G., Besson, F., Blot, E., Guidard, V., Meleux, F., Royer, A., Petiot, V., Miller, C., Fermond, O., Jeant, A., Adani, M., Arteta, J., Benedictow, A., Bergström, R., Bowdalo, D., Brandt, J., Briganti, G., Carvalho, A. C., Christensen, J. H., Couvidat, F., D'Elia, I., D'Isidoro, M., Denier van der Gon, H., Descombes, G., Di Tomaso, E., Douros, J., Escribano, J., Eskes, H., Fagerli, H., Fatahi, Y., Flemming, J., Friese, E., Frohn, L., Gauss, M., Geels, C., Guarnieri, G., Guevara, M., Guion, A., Guth, J., Hänninen, R., Hansen, K., Im, U., Janssen, R., Jeoffrion, M., Joly, M., Jones, L., Jorba, O., Kadantsev, E., Kahnert, M., Kaminski, J. W., Kouznetsov, R., Kranenburg, R., Kuenen, J., Lange, A. C., Langner, J., Lannuque, V., Macchia, F., Manders, A., Mircea, M., Nyiri, A., Olid, M., Pérez García-Pando, C., Palamarchuk, Y., Piersanti, A., Raux, B., Razinger, M., Robertson, L., Segers, A., Schaap, M., Siljamo, P., Simpson, D., Sofiev, M., Stangel, A., Struzewska, J., Tena, C., Timmermans, R., Tsikerdekis, T., Tsyro, S., Tyuryakov, S., Ung, A., Uppstu, A., Valdebenito, A., van Velthoven, P., Vitali, L., Ye, Z., Peuch, V.-H., and Rouïl, L.: Copernicus Atmosphere Monitoring Service – Regional Air Quality Production System v1.0, Geosci. Model Dev., 18, 6835–6883, https://doi.org/10.5194/gmd-18-6835-2025, 2025.

de Meij, A., Cuvelier, C., Thunis, P., Pisoni, E., and Bessagnet, B.: Sensitivity of air quality model responses to emission changes: comparison of results based on four EU inventories through FAIRMODE benchmarking methodology, Geosci. Model Dev., 17, 587–606, https://doi.org/10.5194/gmd-17-587-2024, 2024.

D'Andrimont, R., Verhegghen, A., Lemoine, G., Kempeneers, P., Meroni, M., van der Velde, M.: EUCROPMAP 2018. European Commission, Joint Research Centre (JRC) [Dataset] PID: http://data.europa.eu/89h/15f86c84-eae1-4723-8e00-c1b35c8f56b9, 2021.

Denier van der Gon, H., Janssens-Maenhout, G., Petrescu, A.M.R., Scholze, M., Engelen, R. et al.: The use of prior information in the CO2 Monitoring & Verification Support Capacity for the Copernicus Atmosphere Monitoring Service, European Commission, Ispra, JRC141365, 2025.

EEA: Waterbase – UWWTD: Urban WasteWater Treatment Directive - reported data. Available at: https://www.eea.europa.eu/en/datahub/datahubitem-view/6244937d-1c2c-47f5-bdf1-33ca01ff1715 (last access: September 2024), 2023.

EMEP/EEA: Air pollutant emission inventory guidebook 2023 – Technical guidance to prepare national emission inventories, Publications Office of the European Union, https://data.europa.eu/doi/10.2800/795737, 2023.

https://doi.org/10.5194/egusphere-2026-4146
Preprint. Discussion started: 23 July 2026

European Commission: Directorate-General for Environment, Air quality modelling for air quality policy – Technical support document on the use of modelling for various application domains under the Ambient Air Quality Directive – Final version, Publications Office of the European Union, https://data.europa.eu/doi/10.2779/3343596, 2025.

EU: Regulation (EC) No 166/2006 - EN. - EUR-Lex. https://eur-lex.europa.eu/eli/reg/2006/166/oj/eng, 2006.

EU: Directive - EU – 2024/2881 - EN. - EUR-Lex. https://eur-lex.europa.eu/eli/dir/2024/2881/oj/eng, 2024.

Ferreira, J., Guevara, M., Baldasano, J. M., Tchepel, O., Schaap, M., Miranda, A. I., and Borrego, C.: A comparative analysis of two highly spatially resolved European atmospheric emission inventories, Atmos. Environ., 75, 43–57, https://doi.org/10.1016/j.atmosenv.2013.03.052, 2013.

Gerbig, C., Kaiser-Weiss, A.K., Bovensmann, H., Butterbach-Bahl, K., Plass-Dülmer, and C., Fix, A.: Integrated Greenhouse Gas Monitoring System for Germany (ITMS) - Overall Concept, Version 24.9.2021, available at: https://www.fona.de/de/massnahmen/foerdermassnahmen/ITMS/ITMS_Konzept.pdf?m=1661860754& (last access, August 2025), 2021.

Google: Google Earth Pro, version 7.3.7.1155. Available at: https://www.google.com/earth/about/versions/, (last access: March 2026), 2026.

Grythe, H., Lopez-Aparicio, S., Vogt, M., Vo Thanh, D., Hak, C., Halse, A. K., Hamer, P., and Sousa Santos, G.: The MetVed model: development and evaluation of emissions from residential wood combustion at high spatio-temporal resolution in Norway, Atmos. Chem. Phys., 19, 10217–10237, https://doi.org/10.5194/acp-19-10217-2019, 2019.

Guevara, M., Martínez, F., Arévalo, G., Gassó, S., and Baldasano, J. M.: An improved system for modelling Spanish emissions: HERMESv2.0. Atmos. Environ.. 81, 209–221, https://doi.org/10.1016/j.atmosenv.2013.08.053, 2013.

Guevara, M., Soret, A., Arévalo, G., Martínez, F., and Baldasano J. M.: Implementation of plume rise and its impacts on emissions and air quality modelling, Atmos. Environ., 99, 618-629, DOI: 10.1016/j.atmosenv.2014.10.029, 2014.

Guevara, M., Tena, C., Soret, A., Serradell, K., Guzmán, D., Retama, A., Camacho, P., Jaimes-Palomera, M., and Mediavilla, A.: An emission processing system for air quality modelling in the Mexico City metropolitan area: Evaluation and comparison of the MOBILE6.2-Mexico and MOVES-Mexico traffic emissions, Sci. Total Environ., 584–585, 882–900, https://doi.org/10.1016/j.scitotenv.2017.01.135, 2017.

https://doi.org/10.5194/egusphere-2026-4146
Preprint. Discussion started: 23 July 2026

Guevara, M., Tena, C., Porquet, M., Jorba, O., and Pérez García-Pando, C.: HERMESv3, a stand-alone multi-scale atmospheric emission modelling framework – Part 1: global and regional module, Geosci. Model Dev., 12, 1885–1907, https://doi.org/10.5194/gmd-12-1885-2019, 2019.

Guevara, M., Tena, C., Porquet, M., Jorba, O., and Pérez García-Pando, C.: HERMESv3, a stand-alone multi-scale atmospheric emission modelling framework – Part 2: The bottom–up module, Geosci. Model Dev., 13, 873–903, https://doi.org/10.5194/gmd-13-873-2020, 2020.

Guevara, M., Jorba, O., Tena, C., Denier van der Gon, H., Kuenen, J., Elguindi, N., Darras, S., Granier, C., and Pérez García-Pando, C.: Copernicus Atmosphere Monitoring Service TEMPOral profiles (CAMS-TEMPO): global and European emission temporal profile maps for atmospheric chemistry modelling, Earth Syst. Sci. Data, 13, 367–404, https://doi.org/10.5194/essd-13-367-2021, 2021.

Guevara, M., Enciso, S., Tena, C., Jorba, O., Dellaert, S., Denier van der Gon, H., and Pérez García-Pando, C.: A global catalogue of CO2 emissions and co-emitted species from power plants, including high-resolution vertical and temporal profiles, Earth Syst. Sci. Data, 16, 337–373, https://doi.org/10.5194/essd-16-337-2024, 2024.

Guevara, M., Colette, A., Guion, A., Petiot, V., Adani, M., Arteta, J., Benedictow, A., Bergström, R., Bolignano, A., Camps, P., Carvalho, A. C., Christensen, J. H., Couvidat, F., D'Elia, I., Denier van der Gon, H., Descombes, G., Douros, J., Fagerli, H., Fatahi, Y., Friese, E., Frohn, L., Gauss, M., Geels, C., Hänninen, R., Hansen, K., Jorba, O., Kaminski, J. W., Kouznetsov, R., Kranenburg, R., Kuenen, J., Lannuque, V., Meleux, F., Nyíri, A., Palamarchuk, Y., Pérez García-Pando, C., Robertson, L., Russo, F., Segers, A., Sofiev, M., Struzewska, J., Timmermans, R., Uppstu, A., Valdebenito, A., and Ye, Z.: Technical note: sensitivity of the CAMS regional air quality modelling system to anthropogenic emission temporal variability, Atmos. Chem. Phys., 25, 13245–13278, https://doi.org/10.5194/acp-25-13245-2025, 2025.

Heeley-Hill, A. C., Grange, S.K., Ward, M.W., Lewis, A.C., Owen, N., Jordan, C., Hodgson, G., and Adamson, G.: Frequency of use of household products containing vocs andindoor atmospheric concentrations in homes, Environ. Sci.: Processes Impacts 23,699–713, http://dx.doi.org/10.1039/D0EM00504E, 2021

d'Hondt, J. E. and Petetin, H.: Physics-Constrained Deep Learning for Downscaling Atmospheric Chemistry Simulations: The Role of Auxiliary Forcings and Model Architecture, EGU General Assembly 2026, Vienna, Austria, 3–8 May 2026, EGU26-9829, https://doi.org/10.5194/egusphere-egu26-9829, 2026.

https://doi.org/10.5194/egusphere-2026-4146
Preprint. Discussion started: 23 July 2026

Houyoux, M. R., Vukovich, J. M., Coats Jr., C. J., Wheeler, N. M., and Kasibhatla, P. S.: Emission inventory development and processing for the Seasonal Model for Regional Air Quality (SMRAQ) project, J. Geophys. Rev., 105, 9079–9090, 2000.

IPCC: 2019 Refinement to the 2006 IPCC Guidelines for National Greenhouse Gas Inventories, Calvo Buendia, E., Tanabe, K., Kranjc, A., Baasansuren, J., Fukuda, M., Ngarize, S., Osako, A., Pyrozhenko, Y., Shermanau, P. and Federici, S. (eds). Published: IPCC, Switzerland. Available at: https://www.ipcc-nggip.iges.or.jp/public/2019rf/index.html (last access: 25/10/2025), 2019.

Jähn, M., Kuhlmann, G., Mu, Q., Haussaire, J.-M., Ochsner, D., Osterried, K., Clément, V., and Brunner, D.: An online emission module for atmospheric chemistry transport models: implementation in COSMO-GHG v5.6a and COSMO-ART v5.1-3.1, Geosci. Model Dev., 13, 2379–2392, https://doi.org/10.5194/gmd-13-2379-2020, 2020.

Janssens-Maenhout, G., Pinty, B., Dowell, M., Zunker, H., Andersson, E., Balsamo, G., Bézy, J., Brunhes, T., Bösch, H., Bojkov, B., Brunner, D., Buchwitz, M., Crisp, D., Ciais, P., Counet, P., Dee, D., Denier van der Gon, H., Dolman, H., Drinkwater, M. R., Dubovik, O., Engelen, R., Fehr, T., Fernandez, V., Heimann, M., Holmlund, K., Houweling, S., Husband, R., Juvyns, O., Kentarchos, A., Landgraf, J., Lang, R., Löscher, A., Marshall, J., Meijer, Y., Nakajima, M., Palmer, P. I., Peylin, P., Rayner, P., Scholze, M., Sierk, B., Tamminen, J., and Veefkind, P.: Toward an Operational Anthropogenic CO2 Emissions Monitoring and Verification Support Capacity, Bulletin of the American Meteorological Society, 101(8), E1439-E1451. https://doi.org/10.1175/BAMS-D-19-0017.1, 2020.

Josse, B., Simon, P., and Peuch, V.-H.: Radon global simulations with the multiscale chemistry and transport model MOCAGE, Tellus B: Chemical and Physical Meteorology, 56, 339–356, https://doi.org/10.3402/tellusb.v56i4.16448, 2004.

Kakouri, A., Filippis, G., Korras-Carassa, M.-B., Kuenen, J., Hatzianastassiou, N., Matsoukas, C., and Kontos, T.: AtmoSTEM: A high-resolution spatiotemporal emission model for urban air quality applications, EGU General Assembly 2026, Vienna, Austria, 3–8 May 2026, EGU26-5251, https://doi.org/10.5194/egusphere-egu26-5251, 2026.

Kuenen, J., Dellaert, S., Visschedijk, A., Jalkanen, J.-P., Super, I., and Denier van der Gon, H.: CAMS-REG-v4: a state-of-the-art high-resolution European emission inventory for air quality modelling, Earth Syst. Sci. Data, 14, 491–515, https://doi.org/10.5194/essd-14-491-2022, 2022.

Lin, H., Jacob, D. J., Lundgren, E. W., Sulprizio, M. P., Keller, C. A., Fritz, T. M., Eastham, S. D., Emmons, L. K., Campbell, P. C., Baker, B., Saylor, R. D., and Montuoro, R.: Harmonized Emissions Component (HEMCO) 3.0 as a versatile emissions component for atmospheric models: application in the GEOS-Chem, NASA GEOS, WRF-GC, CESM2, NOAA GEFS-Aerosol, and NOAA UFS models, Geosci. Model Dev., 14, 5487–5506, https://doi.org/10.5194/gmd-14-5487-2021, 2021.

Luo, Q., Segura-Barrero, R., Badia, A., Lauvaux, T., Li, J., Chen, J., and Villalba, G.: Quantifying Urban Biogenic CO2 Fluxes in Greenhouse Gas Budgets: A Scalable Framework and Case Study, EGU General Assembly 2026, Vienna, Austria, 3–8 May 2026, EGU26-2329, https://doi.org/10.5194/egusphere-egu26-2329, 2026.

Ma, S., and Tong, D.Q.: Neighborhood Emission Mapping Operation (NEMO): A 1-km anthropogenic emission dataset in the United States, Sci Data, 9, 680, https://doi.org/10.1038/s41597-022-01790-9, 2022.

Madrid City Council: Traffic data for 2022. Available at: https://datos.madrid.es/portal/site/egob/menuitem.c05c1f754a33a9fbe4b2e4b284f1a5a0/?vgnextoid=33cb30c367e78410VgnVCM1000000b205a0aRCRD&vgnextchannel=374512b9ace9f310VgnVCM100000171f5a0aRCRD&vgnextfmt=default (last access: November 2024), 2024.

Mailler, S., Menut, L., Khvorostyanov, D., Valari, M., Couvidat, F., Siour, G., Turquety, S., Briant, R., Tuccella, P., Bessagnet, B., Colette, A., Létinois, L., Markakis, K., and Meleux, F.: CHIMERE-2017: from urban to hemispheric chemistry-transport modeling, Geosci. Model Dev., 10, 2397–2423, https://doi.org/10.5194/gmd-10-2397-2017, 2017.

Mu, Q., Denby, B. R., Wærsted, E. G., and Fagerli, H.: Downscaling of air pollutants in Europe using uEMEP_v6, Geosci. Model Dev., 15, 449–465, https://doi.org/10.5194/gmd-15-449-2022, 2022.

Murphy, B. N., Nolte, C. G., Sidi, F., Bash, J. O., Appel, K. W., Jang, C., Kang, D., Kelly, J., Mathur, R., Napelenok, S., Pouliot, G., and Pye, H. O. T.: The Detailed Emissions Scaling, Isolation, and Diagnostic (DESID) module in the Community Multiscale Air Quality (CMAQ) modeling system version 5.3.2, Geosci. Model Dev., 14, 3407–3420, https://doi.org/10.5194/gmd-14-3407-2021, 2021.

NAEI: Primary NO_2 emission factors for road transport 2023. Available at: https://naei.energysecurity.gov.uk/emission-factors/emission-factors-transport (last access: June 2024), 2024.

Navarro-Barboza, H., Pandolfi, M., Guevara, M., Enciso, S., Tena, C., Via, M., Yus-Díez, J., Reche, C., Pérez, N., Alastuey, A., Querol, X. and Jorba, O.: Uncertainties in source allocation of carbonaceous aerosols in a Mediterranean region, Environment International, 183, 108252, https://doi.org/10.1016/j.envint.2023.108252, 2024.

https://doi.org/10.5194/egusphere-2026-4146
Preprint. Discussion started: 23 July 2026

Oliveira, K., Guevara, M., Kuenen, J.; Jorba, O., Pérez García-Pando, C. and Denier van der Gon, H: A Comprehensive NMVOC Speciation Database for European Atmospheric Modelling. Sci Data, . https://doi.org/10.1038/s41597-026-07538-z, 2026.

OpenStreetMap contributors: Map of Spain [map]. Extracted by Geofabrik. Available at: https://download.geofabrik.de/europe/spain.html (last access: June 2024), 2024.

Ots, R., Vieno, M., Allan, J. D., Reis, S., Nemitz, E., Young, D. E., Coe, H., Di Marco, C., Detournay, A., Mackenzie, I. A., Green, D. C., and Heal, M. R.: Model simulations of cooking organic aerosol (COA) over the UK using estimates of emissions based on measurements at two sites in London, Atmos. Chem. Phys., 16, 13773–13789, https://doi.org/10.5194/acp-16-13773-2016, 2016.

Pay, M. T., Martínez, F., Guevara, M., and Baldasano, J. M.: Air quality forecasts on a kilometer-scale grid over complex Spanish terrains, Geosci. Model Dev., 7, 1979–1999, https://doi.org/10.5194/gmd-7-1979-2014, 2014.

Piccoli, A., Agresti, V., Bedogni, M., Lonati, G., Pirovano, G.: A bottom-up modelling chain to evaluate the impact of urban road transport policies on air quality and human health, Urban Climate, 55, 101893, https://doi.org/10.1016/j.uclim.2024.101893, 2024.

Pye, H. O. T., Place, B. K., Murphy, B. N., Seltzer, K. M., D'Ambro, E. L., Allen, C., Piletic, I. R., Farrell, S., Schwantes, R. H., Coggon, M. M., Saunders, E., Xu, L., Sarwar, G., Hutzell, W. T., Foley, K. M., Pouliot, G., Bash, J., and Stockwell, W. R.: Linking gas, particulate, and toxic endpoints to air emissions in the Community Regional Atmospheric Chemistry Multiphase Mechanism (CRACMM), Atmos. Chem. Phys., 23, 5043–5099, https://doi.org/10.5194/acp-23-5043-2023, 2023.

Pregger, T. and Friedrich, R.: Effective pollutant emission heights for atmospheric transport modelling based on real-world information, Environmental Pollution, 157, 552-560, https://doi.org/10.1016/j.envpol.2008.09.027, 2009.

Pullinger, M., Zapata-Webborn, E., Kilgour, J., Elam, S., Few, J., Goddard, N., Hanmer, C., McKenna, E., Oreszczyn, T., Webb, L.: Capturing variation in daily energy demand profiles over time with cluster analysis in British homes (September 2019 – August 2022), Applied Energy, 360, 122683, https://doi.org/10.1016/j.apenergy.2024.122683, 2024.

Rodriguez-Rey, D., Guevara, M., Linares, M.P., Casanovas, J., Salmerón, J., Soret, A., Jorba, O., Tena, C. and Pérez García-Pando, C: A coupled macroscopic traffic and pollutant emission modelling system for Barcelona, Transportation Research Part D: Transport and Environment, 92, 102725, https://doi.org/10.1016/j.trd.2021.102725, 2021.

https://doi.org/10.5194/egusphere-2026-4146
Preprint. Discussion started: 23 July 2026

Schiavina, M., Freire, S., Carioli, A. and MacManus, K.: GHS-POP R2023A - GHS population grid multitemporal (1975-2030).European Commission, Joint Research Centre (JRC), doi:10.2905/2FF68A52-5B5B-4A22-8F40-C41DA8332CFE, 2023a.

Schiavina, M., Melchiorri, M., and Pesaresi, M.: GHS-SMOD R2023A - GHS settlement layers, application of the Degree of Urbanisation methodology (stage I) to GHS-POP R2023A and GHS-BUILT-S R2023A, multitemporal (1975-2030)European Commission, Joint Research Centre (JRC), doi:10.2905/A0DF7A6F-49DE-46EA-9BDE-563437A6E2BA, 2023b.

Seemann, S.-L., Daskalakis, N., Qu, K. and Vrekoussis, M.: Combining the Emission Preprocessor HERMES with the Chemical Transport Model TM5-MP, Atmosphere, 15(4), 469, https://doi.org/10.3390/atmos15040469, 2024.

Sič, B., El Amraoui, L., Marécal, V., Josse, B., Arteta, J., Guth, J., Joly, M., and Hamer, P. D.: Modelling of primary aerosols in the chemical transport model MOCAGE: development and evaluation of aerosol physical parameterizations, Geosci. Model Dev., 8, 381–408, https://doi.org/10.5194/gmd-8-381-2015, 2015.

Skipper, T. N., D'Ambro, E. L., Wiser, F. C., McNeill, V. F., Schwantes, R. H., Henderson, B. H., Piletic, I. R., Baublitz, C. B., Bash, J. O., Whitehill, A. R., Valin, L. C., Mouat, A. P., Kaiser, J., Wolfe, G. M., St. Clair, J. M., Hanisco, T. F., Fried, A., Place, B. K., and Pye, H. O. T.: Role of chemical production and depositional losses on formaldehyde in the Community Regional Atmospheric Chemistry Multiphase Mechanism (CRACMM), Atmos. Chem. Phys., 24, 12903–12924, https://doi.org/10.5194/acp-24-12903-2024, 2024.

Soulie, A., Granier, C., Darras, S., Zilbermann, N., Doumbia, T., Guevara, M., Jalkanen, J.-P., Keita, S., Liousse, C., Crippa, M., Guizzardi, D., Hoesly, R., and Smith, S. J.: Global anthropogenic emissions (CAMS-GLOB-ANT) for the Copernicus Atmosphere Monitoring Service simulations of air quality forecasts and reanalyses, Earth Syst. Sci. Data, 16, 2261–2279, https://doi.org/10.5194/essd-16-2261-2024, 2024.

Stockwell, W. R., Kirchner, F., Kuhn, M., and Seefeld, S.: A new mechanism for regional atmospheric chemistry modeling, J. Geophys. Res., 102(D22), 25847–25879, doi:10.1029/97JD00849, 1997.

Tena, C., Gehlen, J., Rizza, L., and Guevara, M.: HERMES_Δ: High-Elective Resolution Modelling Emission System – Delta (Version v1.0.1) [Computer software]. Zenodo. https://doi.org/10.5281/zenodo.21393948, 2026a.

Tena, C., Camps, P., and Guevara, M.: HERMES_Delta Benchmark Dataset [Dataset]. Zenodo. https://doi.org/10.5281/zenodo.21471814, 2026b.

Wu, W., Fu, T.-M., Arnold, S. R., Spracklen, D. V., Zhang, A., Tao, W., Wang, X., Hou, Y., Mo, J., Chen, J., Li, Y., Feng, X., Lin, H., Huang, Z., Zheng, J., Shen, H., Zhu, L., Wang, C., Ye, J., and Yang, X.: Temperature-Dependent Evaporative Anthropogenic VOC Emissions Significantly Exacerbate Regional Ozone Pollution, Environmental Science & Technology, 58, 5430–5441, https://doi.org/10.1021/acs.est.3c09122, 2024.

Yarwood, G., Rao, S., Yocke, M., and Whitten, G.: Updates to the carbon bond chemical mechanism: CB05, Tech. rep., U.S. Environmental Protection Agency, Novato, CA, USA, 2005.

Yarwood, G., Jung, J., Whitten, G., Heo, G., J, M., and M, E.: Updates to the Carbon Bond Mechanism for Version 6 (CB6), in: 9th Annual CMAS Conference, Chapel Hill, NC, 11–13 October 2010, pp. 1–4, 2010.

Zhai, D., van Stiphout, R., Schiavone, G., De Raedt, W., Van Hoof, C.: Characterizing and Modeling Smoking Behavior Using Automatic Smoking Event Detection and Mobile Surveys in Naturalistic Environments: Observational Study, JMIR Mhealth Uhealth, 10(2), e28159, doi: 10.2196/28159, 2022.